

Sublinear Variational Optimization of Gaussian Mixture Models with Millions to Billions of Parameters

Sebastian Salwig^{1,†}, Till Kahlke^{1,†,*}, Florian Hirschberger¹, Dennis Forster² and Jörg Lücke¹

[†]These authors share first authorship on this work.

¹Carl von Ossietzky University Oldenburg, Faculty VI, Machine Learning
Oldenburg, Germany

²Frankfurt University of Applied Sciences, Faculty 3, Data Analytics and AI
Frankfurt am Main, Germany

Abstract

Gaussian Mixture Models (GMMs) range among the most frequently used machine learning models. However, training large, general GMMs becomes computationally prohibitive for datasets with many data points N of high-dimensionality D . For GMMs with arbitrary covariances, we here derive a highly efficient variational approximation, which is integrated with mixtures of factor analyzers (MFAs). For GMMs with C components, our proposed algorithm significantly reduces runtime complexity per iteration from $\mathcal{O}(NCD^2)$ to a complexity scaling linearly with D and remaining constant w.r.t. C . Numerical validation of this theoretical complexity reduction then shows the following: the distance evaluations required for the entire GMM optimization process scale sublinearly with NC . On large-scale benchmarks, this sublinearity results in speed-ups of an order-of-magnitude compared to the state-of-the-art. As a proof of concept, we train GMMs with over 10 billion parameters on about 100 million images, and observe training times of approximately nine hours on a single state-of-the-art CPU.

Keywords: Gaussian Mixture Models, Mixtures of Factor Analyzers, variational optimization, sublinear algorithms, clustering, density estimation, Expectation Maximization

*Corresponding author

email addresses: {sebastian.salwig, till.kahlke, florian.hirschberger, joerg.luecke}@uol.de,
dennis.forster@fb3.fra-uas.de

This is a preliminary version.

1 Introduction

In machine learning and data science, Gaussian Mixture Models (GMMs) are widely used and well-established tools. They are a canonical approach to clustering [1], can provide valuable insight into dataset structures [2], or are used as integral part in conjunction with other approaches for a large diversity of tasks [3–5]. A source of their widespread use is the ability of GMMs to flexibly approximate data densities in potentially high-dimensional data spaces. Hence, any task that can be accomplished by using a parametric data density model can be addressed using an appropriately optimized and sufficiently large GMM. Such generality is possible because GMMs are able to approximate given data densities arbitrarily well [e.g. 6–9], i.e., they are universal probability density estimators.

In the density modelling context, flexible component parametrization and the number of components are crucial for the approximation quality that can be achieved [6, 7]. But if GMMs are applied to the large-scale datasets that are currently used in data science and machine learning, then large numbers of components C get combined with many data points N in potentially very high data dimensions D . In such settings, the optimization of general GMMs quickly becomes computationally infeasible. For instance, the runtime cost for executing a single iteration of standard expectation maximization [EM; 10] scales with $\mathcal{O}(NCD^2)$ for general GMMs, which makes optimization of large-scale models very time consuming or impractical. To address the limited scalability of standard GMM optimization, several lines of research have been pursued. Each such research line aims at a reduction of computational complexity, and in the following different complexity reductions methods are discussed.

A common approach is to constrain the covariances [e.g. 11], e.g. with a strict limitation to only diagonal covariance matrices [12, 13]. Constrained covariances can address the otherwise quadratic scaling with the dimensionality of the data. For instance, if no intra-component correlations are modeled by using diagonal covariance matrices, the cost of one EM iteration is reduced to $\mathcal{O}(NCD)$. However, such constraints make GMMs less flexible, which can, for instance, severely impact their ability to efficiently approximate data densities.

Other approaches to address the quadratic scaling with D include geometrically-oriented approaches [14–16, and references therein], random projections [17], or dimensionality reduction approaches [18–21, and references therein].

Still another line of research that can be applied to reduce the computational cost of GMM optimization aims at reducing the number of data points. Such reduced datasets are known as coresets [e.g. 22–24, and references therein] and replace the set of N original data points by a potentially much smaller weighted set of N' data points. Using the weights generated by a corresponding coreset algorithm, computational efforts only scale with N' . Coresets have been used for GMMs with diagonal covariance matrices [12, 13]. However, for GMMs with more general covariances, a reduction to fewer data points is often not desirable because for data in high-dimensions (large D) sufficiently many data points per component are required to appropriately estimate correlations. Other methods do not directly reduce the number of data points but aim at reducing the computational cost in N by using mini-batching [e.g. 25, 26], training on separate subsets of the dataset [e.g. 27], or by hierarchical training schedules [e.g. 18].

In contrast to approaches mentioned above, we here aim at maintaining as flexible as possible GMMs while still decisively reducing computational complexity. The main contributions of this work can be summarized as follows:

- (A) We derive a truncated variational optimization method [28, 29] applicable to GMMs with arbitrary covariance matrices; and
- (B) We introduce a highly efficient learning algorithm based on Mixtures of Factor Analyzers (MFAs) [18, 30, 31], enabling the application of GMMs with billions of parameters to large-scale datasets.

Additionally, we will make use of advanced seeding approaches [e.g. 32–35, and references therein]. Seeding techniques improve optimization by selecting well-suited initial component centers. But contributions (A) and (B), which jointly define the actual parameter optimization procedure (after initialization) will be the main focus of this work. Our approach enables training of GMMs at scales that were previously considered computationally infeasible.

Regarding research contribution (A), variational optimization is, in general, used to reduce optimization complexity [36, 37], and has repeatedly been applied to mixture models [e.g. 36, 38, 39]. In the case of GMMs with diagonal covariances for components, it has recently been shown [12, 13] that variational optimization can reduce the complexity of one EM iteration from a linear scaling with C to a scaling that is constant w.r.t. C . Such complexity reduction has enabled optimization of the so far largest scale GMMs with up to 50 000 components and millions of parameters. However, existing procedures for reducing computational complexity have only been applied to GMMs with uncorrelated covariances [12, 13]. The derivation rested on the assumption of Euclidean distances in data space and between cluster centers. While this assumption can be motivated if the data within a cluster is uncorrelated, it does not hold for the arbitrary covariances in general GMMs. To address this limitation, we here derive a truncated variational optimization techniques that is directly applicable for GMMs with arbitrary covariance matrices.

Regarding research contribution (B), MFAs allow for a flexible modeling of correlations per component along lower-dimensional hyperplanes. More concretely, each Gaussian component of an MFA model is aligned with a lower-dimensional hyperplane of $H \leq D$ dimensions. The hyperplanes can have arbitrary orientation and can be different for each component. For $H = D$ general GMMs are recovered¹. For many types of data, H can be much smaller than D , however, and the complexity of an EM step is reduced from $\mathcal{O}(NCD^2)$ to $\mathcal{O}(NCDH)$. Because of their reduced complexity in D , MFAs have been shown to be applicable to high dimensional data, where they can accomplish tasks usually reserved for neural network approaches [18]. However, with current optimization techniques, the computational limiting factor of MFAs is their scalability with NC .

By simultaneously reducing how the optimization complexity depends on NC and how it depends on D , we enable the optimization of as flexible as possible GMMs at as large scales as possible. The resulting algorithm, referred to as v-MFA, will be introduced in Sec. 2.

2 Methods

We will first introduce the class of GMMs we consider, i.e., MFAs, and then derive a variational optimization of MFAs in Secs. 2.1 to 2.3. Finally, the implementation of the complete variational EM algorithm is described in Sec. 2.4.

2.1 Variational Optimization of MFAs

In the Mixture of Factor Analyzers (MFA) model [18, 30], a data point $\mathbf{x} \in \mathbb{R}^D$ is modeled by a hidden mixture component $c \in \{1, \dots, C\}$ and a hidden factor $\mathbf{z} \in \mathbb{R}^H$. Each component with mixing proportion π_c (satisfying $\sum_c \pi_c = 1$) and mean $\boldsymbol{\mu}_c \in \mathbb{R}^D$ represents a factor analyzer [1, 31] with a factor loading matrix $\mathbf{\Lambda}_c \in \mathbb{R}^{D \times H}$. The generative model is given by

$$p(c | \Theta) = \pi_c, \quad p(\mathbf{z} | \Theta) = \mathcal{N}(\mathbf{z}; \mathbf{0}, \mathbf{I}), \quad p(\mathbf{x} | \mathbf{z}, c, \Theta) = \mathcal{N}(\mathbf{x}; \mathbf{\Lambda}_c \mathbf{z} + \boldsymbol{\mu}_c, \mathbf{D}_c), \quad (1)$$

where \mathcal{N} represents a multivariate Gaussian distribution, $\mathbf{D}_c := \text{diag}(\sigma_{c,1}^2, \dots, \sigma_{c,D}^2) \in \mathbb{R}^{D \times D}$ is a diagonal matrix containing independent noise, and $\Theta := \{\pi_{1:C}, \mathbf{\Lambda}_{1:C}, \boldsymbol{\mu}_{1:C}, \mathbf{D}_{1:C}\}$ denotes all model parameters.

¹although the GMM is overparameterized in this case

An alternative perspective on the MFA model involves considering it as a GMM with low-rank covariance matrix $\Sigma_c = \Lambda_c \Lambda_c^\top + D_c$. In this case, the generative model is expressed as

$$p(c | \Theta) = \pi_c, \quad p(\mathbf{x} | c, \Theta) = \mathcal{N}(\mathbf{x}; \boldsymbol{\mu}_c, \Lambda_c \Lambda_c^\top + D_c). \quad (2)$$

The reformulation results from marginalization over \mathbf{z} using Gaussian identities.

To fit the MFA model to a given dataset $\mathbf{x}_{1:N}$, we seek parameters $\Theta^* = \operatorname{argmax}_{\Theta} \mathcal{L}(\Theta)$ that optimize the log-likelihood given by

$$\mathcal{L}(\mathbf{x}_{1:N}; \Theta) = \log(p(\mathbf{x}_{1:N} | \Theta)) = \sum_{n=1}^N \log \left(\sum_{c=1}^C \pi_c \mathcal{N}(\mathbf{x}_n; \boldsymbol{\mu}_c, \Lambda_c \Lambda_c^\top + D_c) \right). \quad (3)$$

Direct log-likelihood optimization is usually difficult. Instead, efficient algorithms often employ approaches such as Expectation Maximization (EM) or variational approximations of EM [10, 36, 37]. Variational approaches optimize the free energy, which is a lower bound of the log-likelihood (also known as the evidence lower bound – ELBO). The free energy is iteratively optimized by computing expectation values of latent variables in the E-step and updating the model parameters Θ in the M-step. In this study, we employ a variational version of the EM algorithm, which uses truncated posterior distributions as its family of variational distributions. Concretely, we use variational distributions $q_n(c | \tilde{\Theta})$ defined by

$$\forall n = 1, \dots, N : \quad q_n(c | \tilde{\Theta}) := q(c; \mathbf{x}_n, \mathcal{K}^{(n)}, \tilde{\Theta}) = \frac{p(c, \mathbf{x}_n | \tilde{\Theta})}{\sum_{\tilde{c} \in \mathcal{K}^{(n)}} p(\tilde{c}, \mathbf{x}_n | \tilde{\Theta})} \delta(c \in \mathcal{K}^{(n)}), \quad (4)$$

where $\delta(c \in \mathcal{K}^{(n)})$ is equal to 1 if $c \in \mathcal{K}^{(n)}$ and 0 otherwise (also known as Iverson bracket), and $\mathcal{K}^{(n)}$ denotes those component indices for which the variational distribution $q_n(c | \tilde{\Theta})$ is non-zero. Throughout this work, we will assume that the size of any set $\mathcal{K}^{(n)}$ is restricted to $C' \leq C$ indices, i.e., $|\mathcal{K}^{(n)}| = C'$ for all n .

If we use truncated distributions (Eq. (4)), we obtain as free energy objective

$$\mathcal{F}(\mathbf{x}_{1:N}; \mathcal{K}, \tilde{\Theta}, \Theta) := \sum_{n=1}^N \sum_{c=1}^C q_n(c | \tilde{\Theta}) \log(\pi_c \mathcal{N}(\mathbf{x}_n; \boldsymbol{\mu}_c, \Lambda_c \Lambda_c^\top + D_c)) + \mathcal{H}[q_n], \quad (5)$$

where \mathcal{K} is the collection of all index sets $\mathcal{K}^{(n)}$ and $\mathcal{H}[q_n] = -\sum_n \mathbb{E}_{q_n}[\log q_n(c | \tilde{\Theta})]$ is the Shannon entropy. The ‘hard’ zeros used by the truncated distributions mean that all sums over components C effectively only have to evaluate C' non-zero summands. This reduces the computational complexity of one M-step from linearly scaling with C to a linear scaling with C' .

The optimal values of the variational parameters $\tilde{\Theta}$ are the current values of the model parameters Θ , which can be shown in general [40] and which, therefore, also applies for the MFA model. For $\tilde{\Theta} = \Theta$ the free energy simplifies to (compare, e.g., [29, 40]):

$$\mathcal{F}(\mathcal{K}, \Theta) := \mathcal{F}(\mathbf{x}_{1:N}; \mathcal{K}, \Theta, \Theta) = \sum_{n=1}^N \log \left(\sum_{c \in \mathcal{K}^{(n)}} p(c, \mathbf{x}_n | \Theta) \right). \quad (6)$$

As can be seen by considering Eq. (6), optimizing the MFA model using variational EM requires to repeatedly evaluate joint probabilities $p(c, \mathbf{x}_n | \Theta)$ or, equivalently, log-joints. In previous work [12, 13], the use of GMMs with diagonal covariance matrices enabled the evaluation of a single log-joint in $\mathcal{O}(D)$. However, in this work, the goal is to model correlations, which substantially increases the computational complexity to $\mathcal{O}(D^2)$ when all correlations are considered. By modeling data distributions along lower-dimensional hyperplanes, the MFA model reduces the complexity to $\mathcal{O}(DH)$ while still preserving correlations. Further details on the computational techniques employed for the MFA model, as well as the derivations of the parameter updates, can be found in Appendices A.1 and A.2, respectively.

2.2 Efficient Partial Variational E-steps

As with other variational approaches, the crucial challenge is to derive a computationally efficient E-step. To do so for the MFA model, we follow here a strategy similar to previous work [12, 13], which has derived efficient partial variational E-steps focusing on diagonal covariance matrices.

We start by noting that the joint probabilities defined by the MFA model play a central role in the optimization of the free energy. This role is underlined by the following proposition:

Proposition 1: Consider the joint probability $p(c, \mathbf{x}_n | \Theta)$ defined by the MFA generative model in Eq. (2), and the free energy \mathcal{F} for index sets \mathcal{K} . If we replace a component $c \in \mathcal{K}^{(n)}$ by a component $\tilde{c} \notin \mathcal{K}^{(n)}$ (for an arbitrary n), then the free energy increases if and only if $p(\tilde{c}, \mathbf{x}_n | \Theta) > p(c, \mathbf{x}_n | \Theta)$.

Proposition 1 is a special case of a general result for truncated variational distributions [40]. It therefore applies to any mixture model and to MFA as a special case. For completeness, we provide the proof for general mixture models in Appendix A.3.

Proposition 1 then leads to an equivalent definition of the optimal variational parameters $\mathcal{K}^{(n)}$ as in previous work [12, 13]. $\mathcal{K}_{\text{opt}}^{(n)}$ is given by

$$\mathcal{K}_{\text{opt}}^{(n)} = \{c \mid p(c, \mathbf{x}_n | \Theta) \text{ is among the } C' \text{ largest joints}\}, \quad (7)$$

i.e., the optimal sets $\mathcal{K}_{\text{opt}}^{(n)}$ contain those C' components with the highest joint probabilities (also compare [38, 39]). However, finding the optimal components would require the evaluation of C' joints per data point, i.e., NC joint evaluations in total. Hence, finding the optimal $\mathcal{K}^{(n)}$ given by Eq. (7) would require the same number of joint evaluations as a full E-step. To also reduce the computational complexity of the E-step, we consequently seek a procedure similar to [12, 13], that builds upon partial variational E-steps, i.e., we seek an increase of the free energy instead of its maximization. In virtue of Proposition 1, we can increase the free energy by identifying components with *higher* joints rather than finding the C' components with the *highest* joints. This can be accomplished efficiently by evaluating only a subset of all joint probabilities during each E-step, which reduces the computational load compared to a full E-step. Concretely, similar to [12], we introduce a set $\mathcal{S}^{(n)}$, referred to as the search space², that includes candidate components \tilde{c} which may replace a $c \in \mathcal{K}^{(n)}$ to increase the free energy for each data point \mathbf{x}_n . The size of $\mathcal{S}^{(n)}$ is upper-bounded, i.e., we demand for all n that $|\mathcal{S}^{(n)}| \leq S$. Here, S will be chosen to be larger than C' but significantly smaller than C (i.e., $C' < S \ll C$). Instead of finding the *optimal* sets $\mathcal{K}_{\text{opt}}^{(n)}$, we now partially optimize each $\mathcal{K}^{(n)}$ using the search space $\mathcal{S}^{(n)}$ of a given \mathbf{x}_n . Given $\mathcal{S}^{(n)}$ the updated $\mathcal{K}^{(n)}$ is defined by:

$$\mathcal{K}^{(n)} = \{c \mid p(c, \mathbf{x}_n | \Theta) \text{ is among the } C' \text{ largest joints for all } c \in \mathcal{S}^{(n)}\}. \quad (8)$$

The index set $\mathcal{K}^{(n)}$ of Eq. (8) can consequently be determined by evaluating all joints with \mathbf{x}_n and all $c \in \mathcal{S}^{(n)}$ as arguments.

We will define each search space $\mathcal{S}^{(n)}$ to contain $\mathcal{K}^{(n)}$ as subset ($\mathcal{K}^{(n)} \subset \mathcal{S}^{(n)}$), which guarantees that the update of $\mathcal{K}^{(n)}$ according to Eq. (8) never decreases the free energy $\mathcal{F}(\mathcal{K}, \Theta)$. However, this condition on the search spaces $\mathcal{S}^{(n)}$ is not sufficient to warrant an efficient increase of the free energy. For a high efficiency, components $\tilde{c} \in \mathcal{S}^{(n)}$ that are not in $\mathcal{K}^{(n)}$ have to be likely to result in larger joints, i.e., it has to be sufficiently likely for $\tilde{c} \in \mathcal{S}^{(n)}$ that $p(\tilde{c}, \mathbf{x}_n | \Theta) > p(c, \mathbf{x}_n | \Theta)$ with $\tilde{c} \notin \mathcal{K}^{(n)}$ and $c \in \mathcal{K}^{(n)}$.

A first trivial option to define $\mathcal{S}^{(n)}$ would be to use all $c \in \mathcal{K}^{(n)}$ as members of $\mathcal{S}^{(n)}$, and to then add component indices that are uniformly sampled from $\{1, \dots, C\}$. However, as C increases, the probability of finding a new component \tilde{c} with high joint $p(\tilde{c}, \mathbf{x}_n | \Theta)$ becomes increasingly small. Therefore, we seek an approach that suggests components \tilde{c} that are more likely to increase the free energy than such a blind random search.

²The search space is denoted as \mathcal{G}_n in [12].

2.3 Construction of the search space for guided search

In order to allow for a more guided search, we will define the search spaces $\mathcal{S}^{(n)}$ to contain component indices likely to improve the free energy while being still efficiently computable. We remain with a data point centric approach and use a bootstrapping strategy to continuously improve the search spaces $\mathcal{S}^{(n)}$ together with the sets $\mathcal{K}^{(n)}$. In line with previous research [12], we define the search spaces $\mathcal{S}^{(n)}$ by making use of (data point independent) sets g_c , that contain replacement candidates for c . However, in this work, the definition of these sets will be introduced in a novel manner to account for GMMs with arbitrary covariances. The components $\tilde{c} \in g_c$ can, for now, be thought of as components estimated to be ‘similar’ to component c but we will only precisely define the g_c further below. Using the sets g_c , a search space $\mathcal{S}^{(n)}$ for a given data point is defined as the following union:

$$\mathcal{S}^{(n)} := \bigcup_{c \in \mathcal{K}^{(n)}} g_c. \quad (9)$$

To ensure that the size of the search space is upper bounded, we restrict the maximum size of the sets g_c to G . The maximum size of a search space $\mathcal{S}^{(n)}$ is thus reached in the case when all g_c are disjoint (in that case its size is given by $S = |\mathcal{K}^{(n)}| |g_c| = C'G$). In general the index sets g_c may intersect, however, leading to smaller $\mathcal{S}^{(n)}$.

The construction of the search space by Eq. (9) can be conceptualized as a search tree structure. Specifically, we build $\mathcal{S}^{(n)}$ by first considering all components in $\mathcal{K}^{(n)}$, which contains the most relevant components identified so far for \mathbf{x}_n . Next, for each component $c \in \mathcal{K}^{(n)}$, we consider the set of components in g_c , that provides replacement candidates for component c . Fig. 1 offers an illustration of the sets g_c and the construction of $\mathcal{S}^{(n)}$. Fig. 1A shows a schematic representation, Fig. 1B visualize $\mathcal{K}^{(n)}$ and g_c , and Fig. 1C illustrates $\mathcal{S}^{(n)}$ in data space. Fig. 1 also demonstrates that $|\mathcal{S}^{(n)}|$ is larger than $|\mathcal{K}^{(n)}|$ but significantly smaller than C .

It remains to define the sets g_c . In previous work [12], the sets g_c were updated based on Euclidean neighborhoods. Concretely, a set g_c contained components \tilde{c} with small Euclidean distances $\|\boldsymbol{\mu}_c - \boldsymbol{\mu}_{\tilde{c}}\|$ to the component c (with $\boldsymbol{\mu}_c$ and $\boldsymbol{\mu}_{\tilde{c}}$ denoting component centers). These component-to-component distances were then approximated using component-to-datapoint distances (for further details, see [12]).

In our case, however, covariance matrices are not restricted to the uncorrelated case. The general and potentially strong correlations we seek to model can strongly change proximity relations among components as well as between data points and components, which makes previous Euclidean distance metrics [12, 13] unsuitable for finding relevant components for a given component. Fig. 2 highlights that for general covariance matrices, small distances no longer correspond to large joint values.

Instead of finding components similar to component c using Euclidean distances, we measure component similarities via the Kullback-Leibler (KL) divergence. The KL-divergence between the probability distributions of a component c and component \tilde{c} is given by:

$$D_{\text{KL}} [p(\mathbf{x} | c, \boldsymbol{\Theta}) || p(\mathbf{x} | \tilde{c}, \boldsymbol{\Theta})] = \mathbb{E}_{p(\mathbf{x} | c, \boldsymbol{\Theta})} \left[\log \frac{p(\mathbf{x} | c, \boldsymbol{\Theta})}{p(\mathbf{x} | \tilde{c}, \boldsymbol{\Theta})} \right]. \quad (10)$$

Although there exists an analytically tractable form of the KL-divergence for Gaussian distributions, evaluating Eq. (10) introduces additional computational overhead, and the divergence has to be computed for all (c, \tilde{c}) pairs. Thus, we aim to efficiently estimate the KL-divergence, while still capturing sufficient information about the KL-divergences for those (c, \tilde{c}) pairs that are relevant for the optimization algorithm. To achieve this, we employ a finite sample approximation of Eq. (10). Instead of drawing samples from $p(\mathbf{x} | c, \boldsymbol{\Theta})$, we estimate the KL-divergence by using the data points currently assigned to component c . This gives rise to the introduction of a partitioning of the dataset into the following sets:

$$\mathcal{I}_c = \{n | c = c_n\} \quad \text{with} \quad c_n = \underset{c' \in \mathcal{K}^{(n)}}{\operatorname{argmax}} p(c' | \mathbf{x}_n, \boldsymbol{\Theta}) = \underset{c' \in \mathcal{K}^{(n)}}{\operatorname{argmax}} p(c', \mathbf{x}_n | \boldsymbol{\Theta}). \quad (11)$$

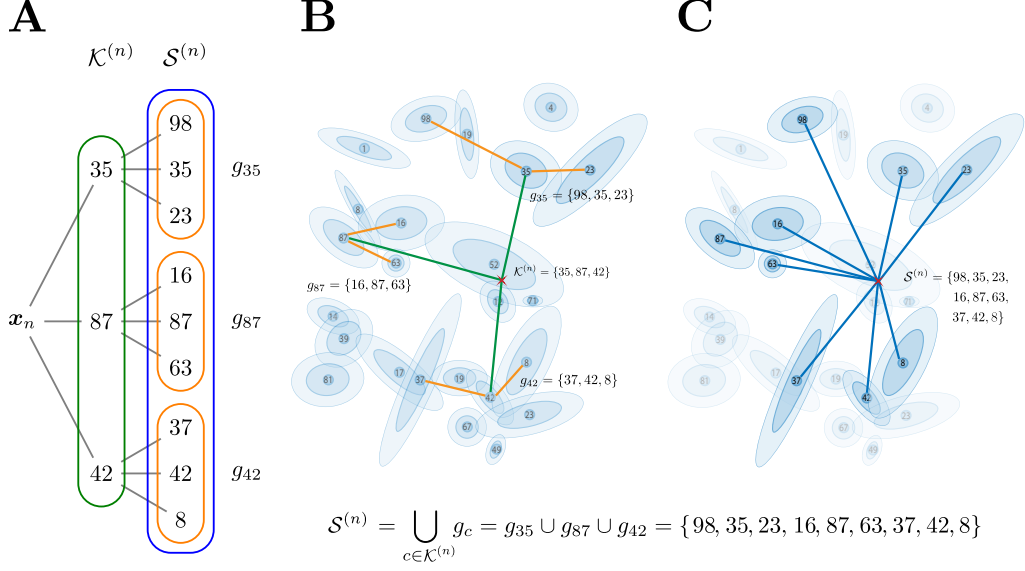


Figure 1: Construction of $\mathcal{S}^{(n)}$ for a data point \mathbf{x}_n . Subfigure **A** shows a schematic representation while **B** visualizes $\mathcal{K}^{(n)}$ and g_c , and **C** visualizes $\mathcal{S}^{(n)}$ in data space. In this example, the set $\mathcal{K}^{(n)} = \{35, 87, 42\}$ contains $C' = 3$ component indices for \mathbf{x}_n , as indicated by the green box in **A** and green lines in **B**. Each of the three components has a set of neighborhoods g_c that includes the component c itself and two additional component indices, i.e., $|g_c| = G = 3$. Specifically, we have $g_{35} = \{98, 35, 23\}$, $g_{87} = \{16, 87, 63\}$ and $g_{42} = \{37, 42, 8\}$. These three sets are highlighted by orange boxes in **A** and orange lines in **B**. The union of the three sets g_c forms the search space $\mathcal{S}^{(n)} = \{98, 35, 23, 16, 87, 63, 37, 42, 8\}$, as indicated by the blue box in **A** and blue lines in **C**. None of the sets are optimal for the data point \mathbf{x}_n yet. The optimization procedure will be explained in the following.

Given the sets \mathcal{I}_c , the KL-divergence between the probability distributions of a component c and \tilde{c} can be estimated as follows (see Appendix A.4 for details):

$$D_{\text{KL}} [p(\mathbf{x} | c, \Theta) || p(\mathbf{x} | \tilde{c}, \Theta)] \approx \frac{1}{N_{c\tilde{c}}} \sum_{n \in \mathcal{I}_c} \log \frac{p(\mathbf{x}_n | c, \Theta)}{p(\mathbf{x}_n | \tilde{c}, \Theta)} \delta(\tilde{c} \in \mathcal{S}^{(n)}) =: D_{c\tilde{c}} \quad (12)$$

where $N_{c\tilde{c}} = \sum_{n \in \mathcal{I}_c} \delta(\tilde{c} \in \mathcal{S}^{(n)})$.

If we disregard the condition $\delta(\tilde{c} \in \mathcal{S}^{(n)})$, the function $D_{c\tilde{c}}$ estimates the KL-divergence using *all* data points in \mathcal{I}_c . The condition $\delta(\tilde{c} \in \mathcal{S}^{(n)})$, however, reduces the number of samples to approximate the KL-divergence by considering only those data points for which component \tilde{c} is present in their search spaces. Due to $\delta(\tilde{c} \in \mathcal{S}^{(n)})$ in Eq. (12), the function $D_{c\tilde{c}}$ is defined only for a restricted subset of components \tilde{c} . For those \tilde{c} that do not appear in any of the search spaces, (i.e., any $\tilde{c} \notin \bigcup_{n \in \mathcal{I}_c} \mathcal{S}^{(n)}$), we set $D_{c\tilde{c}}$ to infinity, formally treating the component \tilde{c} for c as irrelevant.

Eq. (12) yields a ranking where a lower value of $D_{c\tilde{c}}$ indicates a greater similarity of component \tilde{c} to c . Consequently, we can define g_c as the set of those components that result in the G lowest values of $D_{c\tilde{c}}$, i.e.,

$$g_c = \{\tilde{c} \mid D_{c\tilde{c}} \text{ is among the } G \text{ lowest values}\}. \quad (13)$$

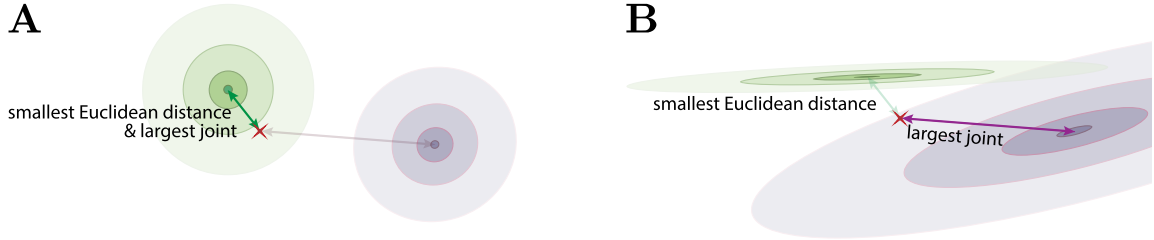


Figure 2: Comparison of Euclidean distances and joints. In **A** and **B**, the component centers are identical and the same data point is marked with a red cross. For isotropic, equally weighted components (**A**), the smallest Euclidean distance correspond to largest joint between components and the data point. However, for general covariance matrices (**B**), this is no longer the case.

The definition of $D_{c\tilde{c}}$ in Eq. (12) ensures that no additional computations of $p(\mathbf{x}_n | \tilde{c}, \Theta)$ are required beyond those that anyway have to be performed in a partial E-step (see Sec. 2.4 for details). As a result, $D_{c\tilde{c}}$, and thus the sets g_c , are consequently very efficiently computable. A potential drawback is that $D_{c\tilde{c}}$ may only provide a coarse estimate of the KL-divergence, depending on the convergence state of the search spaces, the model parameters, etc. (we elaborate in Appendix A.4). Importantly, however, the estimate still captures sufficient information about component similarities in the sense of KL-divergences. Since we only require the values of $D_{c\tilde{c}}$ to rank components \tilde{c} , their exact values are of secondary importance.

We note that a relation to KL-divergences was also discussed in [12]. However, the general distance introduced in [12] was approximated in such a way that, for isotropic GMMs, it recovers a measure based on Euclidean distances. Further details, along with numerical comparisons to our novel and generalized method, are provided in Appendices A.4.1 and B.2.1. While the here defined method (based on Eq. (12)) is especially advantageous in the general case with intra-component correlations, we also observed improvements for the uncorrelated case.

2.4 Algorithmic Realization of v-MFA

While Secs. 2.1 to 2.3 described the theoretical foundation of the variational learning algorithm for MFA models, we now focus on its algorithmic realization (which we will refer to as v-MFA). Analogously to conventional EM optimization, v-MFA alternates between E-steps and M-steps to update variational parameters and model parameters, respectively. The variational E-step is discussed below, and details on the M-step are provided in Appendix A.2.

Variational E-step: Alg. 1 shows the partial variational E-step, which comprises four blocks (variables are implicitly initialized with zeros or empty sets, respectively):

- (1) For each data point, the search space $\mathcal{S}^{(n)}$ is constructed and a component, drawn from a discrete uniform distribution $\mathcal{U}\{1, C\}$, is added to $\mathcal{S}^{(n)}$ (it consequently applies that $|\mathcal{S}^{(n)}| \leq C'G + 1$). Subsequently, the joints are evaluated for all $c \in \mathcal{S}^{(n)}$. The $\mathcal{K}^{(n)}$ sets are then optimized using these joints. Fig. 3 visualizes the iterative procedure for $\mathcal{K}^{(n)}$ optimization.
- (2) The partition $\mathcal{I}_{1:C}$ of the dataset is computed.
- (3) The partition and the previously computed joints are used to determine the sets $g_{1:C}$, utilizing $\log p(\mathbf{x}_n | c, \Theta) = \log p(c, \mathbf{x}_n | \Theta) - \log p(c | \Theta)$. $D_{c\tilde{c}} = \tilde{D}_{c\tilde{c}}/N_{c\tilde{c}}$ will be computed for all $\tilde{c} \in \bigcup_{n \in \mathcal{I}_c} \mathcal{S}^{(n)}$ excluding $\tilde{c} = c$, because c will always be included in g_c .
- (4) The variational distributions $q_n(c | \Theta)$ are computed by normalizing of $p(c, \mathbf{x}_n | \Theta)$.

The computational complexity of a single variational E-step is $\mathcal{O}(NSDH)$, dominated by the joint computations in block 1 (assuming $N > C$). Unlike conventional E-steps, which require evaluating NC joint

Algorithm 1: Variational E-step

```
for  $n = 1 : N$  do
   $\mathcal{S}^{(n)} = \bigcup_{c \in \mathcal{K}^{(n)}} g_c$ ;
   $\mathcal{S}^{(n)} = \mathcal{S}^{(n)} \cup \{c\}$  with  $c \sim \mathcal{U}\{1, C\}$ ;
  for  $c \in \mathcal{S}^{(n)}$  do
    compute joint  $p(c, \mathbf{x}_n | \Theta)$ ;
   $\mathcal{K}^{(n)} = \{c | p(c, \mathbf{x}_n | \Theta) \text{ is among the } C' \text{ largest joints for all } c \in \mathcal{S}^{(n)}\}$ ;

for  $n = 1 : N$  do
   $c_n = \operatorname{argmax}_{c \in \mathcal{K}^{(n)}} p(c, \mathbf{x}_n | \Theta)$ ;
   $\mathcal{I}_{c_n} = \mathcal{I}_{c_n} \cup \{n\}$ ;

for  $c = 1 : C$  do
  for  $n \in \mathcal{I}_c$  do
    for  $\tilde{c} \in \mathcal{S}^{(n)} \setminus \{c\}$  do
       $\tilde{D}_{c\tilde{c}} = \tilde{D}_{c\tilde{c}} + \log p(\mathbf{x}_n | c, \Theta) - \log p(\mathbf{x}_n | \tilde{c}, \Theta)$ ;
       $N_{c\tilde{c}} = N_{c\tilde{c}} + 1$ ;
     $g_c = \{\tilde{c} | \tilde{D}_{c\tilde{c}}/N_{c\tilde{c}} \text{ is among the } G - 1 \text{ smallest values of all computed } \tilde{D}_{c\tilde{c}}/N_{c\tilde{c}}\} \cup \{c\}$ ;

for  $n = 1 : N$  do
  for  $c \in \mathcal{K}^{(n)}$  do
     $q_n(c | \Theta) = p(c, \mathbf{x}_n | \Theta) / \sum_{\tilde{c} \in \mathcal{K}^{(n)}} p(\tilde{c}, \mathbf{x}_n | \Theta)$ ;
```

probabilities by considering combinations of all data points with all components, the variational E-step only loops over all data points and their respective search spaces. As a result, it requires at most NS joint evaluations, which is significantly fewer when $S \ll C$. A detailed specification of the complexity is provided in Appendix A.5.

Initialization of model parameters: To preserve the algorithmic complexity of Alg. 1, initialization methods should exhibit complexities that are comparable or lower than those of the optimization algorithm itself. The k -means++ seeding method [32] is not suitable in our context, for instance, because it scales with $\mathcal{O}(NCD)$. Therefore, we employ AFK-MC² [34] as an efficient initialization method for initial values for the means $\boldsymbol{\mu}_c$. To initialize the diagonal variances $\mathbf{D}_{1:C}$, we compute the variance along each dimension across all data points as follows:

$$\mathbf{D}_c = \mathbf{D}_{\text{init}} \quad \forall c \quad \text{with } \mathbf{D}_{\text{init}} = \operatorname{diag}(\sigma_1^2, \dots, \sigma_D^2) \text{ and } \sigma_d^2 = \operatorname{var}(x_{1:N,d}), \quad (14)$$

where $x_{n,d}$ is the d -th entry of \mathbf{x}_n . Regarding the factor loading matrices $\mathbf{\Lambda}_c$, we used uniform random numbers between 0 and 1 to set their values. Initialization methods proposed by [18, 31] are computationally too demanding for our specific setting.

Initialization of variational parameters: The initialization of index sets $\mathcal{K}_{1:N}$ and $g_{1:C}$ proceeds as follows: Data points designated as seeds for components, sampled by AFK-MC², ensure that the corresponding component index is contained within the respective set \mathcal{K}_n . The set g_c consistently includes index c . Subsequently, $\mathcal{K}_{1:N}$ and $g_{1:C}$ are populated with further indices by sampling uniformly from $\{1, \dots, C\}$ (while ensuring uniqueness of the indices). Following this, $\mathcal{K}_{1:N}$ and $g_{1:C}$ are optimized through initial partial E-steps, while keeping the model parameters fixed. This approach has been previously shown to yield favorable results [12]. We refer to this procedure as *warm-up*.

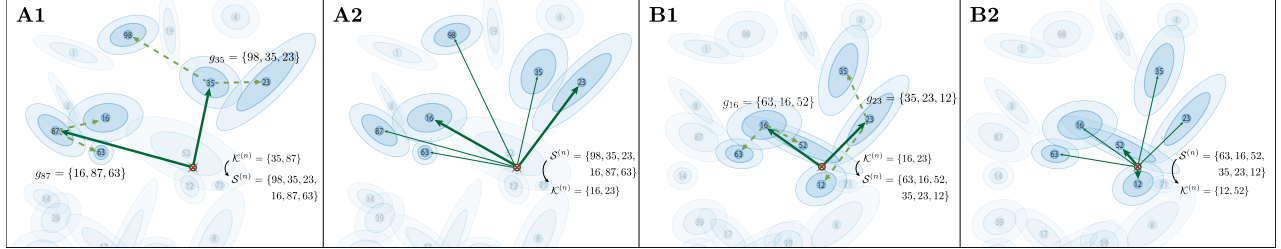


Figure 3: Update of $\mathcal{K}^{(n)}$ over two iterations. In **A1**, a red cross marks a data point \mathbf{x}_n with an initial suboptimal $\mathcal{K}^{(n)} = \{35, 87\}$ (we are here for simplicity only using $C' = 2$) and $G = 3$ replacement candidates for each of those components: $g_{35} = \{98, 35, 23\}$ and $g_{87} = \{16, 87, 63\}$. Also these replacement candidates are still suboptimal. Subsequently, in **A2**, the joints $p(c, \mathbf{x}_n | \Theta)$ to all components in the search space $\mathcal{S}^{(n)} = g_{35} \cup g_{87} = \{98, 35, 23, 16, 87, 63\}$ are calculated, and the $C' = 2$ components with largest joints are selected as new $\mathcal{K}^{(n)} = \{16, 23\}$. In the following steps of the algorithm, the replacement candidates g_c will be adjusted based on the current $\mathcal{S}^{(n)}$, and the model parameters will be updated in the M-step. In **B1** and **B2** the same procedure is repeated in the next iteration to find components $\mathcal{K}^{(n)}$ with larger joints. In this example, over two iterations, a total of 12 joints were calculated to find the best final $\mathcal{K}^{(n)}$, which is only a fraction of the total number of calculations required had we considered all C components.

Complete v-MFA: The implementation of the complete v-MFA algorithm is outlined in Alg. 2. Following initialization, the algorithm performs variational E-steps in a *warm-up* phase until the free energy $\mathcal{F}(\mathcal{K}, \Theta)$ has converged. Subsequently, the main training process alternates between variational E-steps and M-steps until $\mathcal{F}(\mathcal{K}, \Theta)$ has converged again. As convergence criterion for both loops, we consider $\mathcal{F}(\mathcal{K}, \Theta)$ to have converged after iteration t if

$$\frac{\mathcal{F}^{(t)} - \mathcal{F}^{(t-1)}}{\mathcal{F}^{(t-1)}} < \varepsilon, \quad (15)$$

where $\mathcal{F}^{(t)}$ is the free energy $\mathcal{F}(\mathcal{K}, \Theta)$ of Eq. (6) at iteration t (cf. [12]). In all numerical experiments we choose the convergence threshold $\varepsilon = 10^{-4}$ unless specifically stated otherwise.

Algorithm 2: v-MFA

initialize $\pi_{1:C}, \boldsymbol{\mu}_{1:C}, \boldsymbol{\Lambda}_{1:C}, \mathbf{D}_{1:C}, \mathcal{K}_{1:N}$ and $g_{1:C}$ (see text for details);
repeat
1 | *variational E-step:* update $\mathcal{K}_{1:N}, g_{1:C}$ using Alg. 1;
until $\mathcal{F}(\mathcal{K}, \Theta)$ has converged;

repeat
2 | *variational E-step:* update $\mathcal{K}_{1:N}, g_{1:C}$ using Alg. 1;
| *variational M-step:* update $\pi_{1:C}, \boldsymbol{\mu}_{1:C}, \boldsymbol{\Lambda}_{1:C}$ and $\mathbf{D}_{1:C}$ (see Appendix A.2 for details);
until $\mathcal{F}(\mathcal{K}, \Theta)$ has converged;

3 Results

To assess the efficiency and effectiveness of the v-MFA algorithm, we conducted a series of numerical experiments organized into three sections. In Sec. 3.1, we provide a comprehensive comparison of the scaling behavior

with increasing component numbers C of the v-MFA algorithm to conventional EM optimization of MFA models, referred to as em-MFA. Here, the em-MFA algorithm serves as a canonical baseline. Following the scaling analysis, we evaluate in Sec. 3.2 the performance and quality of the v-MFA algorithm relative to em-MFA. We also compare the v-MFA algorithm to a k -means algorithm combined with factor analyzers, denoted as k -means+FA (see Sec. 3.2). Finally, in Sec. 3.3, we extend the analysis to dataset and model sizes where the application of em-MFA is no longer feasible. On such tasks the efficiency of v-MFA translates to its ability to train GMMs at scales that have previously not been reported. Further details on the numerical experiments are provided in Appendix B.1 and complementary control experiments are reported in Appendix B.2.

We evaluated v-MFA on four well-established benchmarks for high-dimensional image data, namely CIFAR-10 [41], CelebA [42], EMNIST [43] and SVHN [44]. The datasets have frequently been applied in different contexts, and they were used previously in settings similar to the one of interest here [12, 13, 18]. The main properties of the datasets are listed in Tab. 1, and details are provided in Appendix B.1.3. Image data is commonly used for benchmarking, and is often considered as an example for data points lying close to a data manifold with much lower dimension than the dimensionality of the data. Images are consequently well suited to assess the effectiveness and efficiency of algorithms that optimize MFA approximations of GMM data models. Moreover, the chosen datasets provide a sufficiently large number of data points to estimate components for the large-scale MFA models we are interested in.

Table 1: High-dimensional datasets used in our experiments. The data dimension is given in pixel width \times pixel height \times color channels.

dataset		train samples	test samples	data dimension D
CIFAR-10	[41]	50 000	10 000	$32 \times 32 \times 3 = 3072$
CelebA	[42]	182 637	19 962	$64 \times 64 \times 3 = 12\,288$
EMNIST	[43]	697 932	116 323	$28 \times 28 \times 1 = 784$
SVHN	[44]	604 388	26 032	$32 \times 32 \times 3 = 3072$

In the numerical experiments, we evaluated the efficiency of v-MFA and corresponding baselines in different settings using two measures for computational costs: the total number of joint probability evaluations (treated as generalized distances) and the wall-clock runtime (compare [12, 13]).

The first measure, the total number of joint evaluations, is independent of concrete implementation details and the hardware used. The number of joint evaluations also excludes initialization, parameter updates within the M-steps and auxiliary computations. The second measure, the wall-clock runtime, encompasses all computations, memory management, and other auxiliary routines. Actual improvements in wall-clock runtimes hold significant practical relevance, albeit this measure is inherently contingent upon implementation details and the hardware used.

For the models under consideration, we can assess the algorithms’ effectiveness using the negative log-likelihood (NLL), which represents a canonical quality measure for probabilistic models. In experimental settings where the em-MFA algorithm can be used as a reference, we employ the relative NLL given by

$$\text{rel. NLL} = \frac{\text{NLL}_{\text{algo}} - \text{NLL}_{\text{em-MFA}}}{\text{NLL}_{\text{em-MFA}}}, \quad (16)$$

where NLL_{algo} refers to the NLL of the respective algorithm (e.g., v-MFA), and where $\text{NLL}_{\text{em-MFA}}$ is the NLL of the em-MFA algorithm. Distance-based metrics that do not account for correlations within components (such as the quantization error used for k -means) are much less appropriate for our analysis.

3.1 Scalability

The v-MFA algorithm, which was derived in Sec. 2.1, exhibits a reduced algorithmic complexity per iteration compared to the em-MFA algorithm. However, the question arises if the much reduced complexity of v-MFA in a single iteration results in a reduced complexity for the entire training process. If increasingly many iterations would be necessary, the gain in efficiency per iteration would be negated. Furthermore, v-MFA requires initial E-steps and updating of search spaces $\mathcal{S}^{(n)}$ and sets g_c during partial E-steps, which results in additional computations compared to em-MFA.

To investigate the scalability of v-MFA compared to em-MFA, we measured the computational demands (per data point) of both algorithms as the number of mixture components C increases. Commonly, an increase in the number of model parameters requires a corresponding increase in the amount and complexity of the data to effectively train the model. Maintaining a constant dataset size while increasing C could simplify the optimization task: typically, the number of iterations until convergence reduces if the ratio of data points to model parameters is reduced. To mitigate this effect, we have chosen to simultaneously increase the size of the datasets when we increase C . These datasets were constructed as follows: for each value of C we evaluated, we uniformly subsampled \tilde{N} data points, where \tilde{N} was determined based on the total dataset size N and the ratio of the current value C to the maximum value C_{\max} investigated, i.e., $\tilde{N} = N \cdot C / C_{\max}$. This approach maintains a constant ratio of \tilde{N}/C for each C , with the consequence that the number of iterations required until convergence changes only slightly as C is increased. For the largest value of C (i.e., $C = C_{\max}$) the entire dataset was used. Note that the evaluation of scalability is different in detail from previous evaluations [e.g. 12]. But also in our case we changed the dataset size with C in order to measure the efficiency independently of secondary effects on the number of required iterations.

To investigate scalability, we applied v-MFA and em-MFA to all four benchmark datasets (see Tab. 1) for different numbers of components C . Specifically, for each dataset and algorithm, we varied the number of components from $C = 100$ to 800 in steps of 100. We fixed the hyperplane dimensionality to $H = 5$. For v-MFA we used the same setting ($C' = 3$ and $G = 15$) for the approximation parameters for all four datasets and all component numbers (other settings we investigate in Sec. 3.2). Each algorithm was executed until the convergence criterion was reached (see Eq. (15)). The result of the scalability analysis is summarized in Fig. 4.

To quantify the scalability of v-MFA and em-MFA with C , we fitted regressions of the form $f(C) = bC^a$. This corresponds to a linear function $\log(f(C)) = \tilde{b} + a \log(C)$ in log-log plots. Hence, the slopes of the straight lines in Fig. 4 provide the scaling exponent for C .

For em-MFA, each iteration requires precisely NC joint evaluations, hence C joint evaluations per data point. Additionally, the number of iterations tends to increase slightly as the number of components C increases, as also previously observed [e.g. 12]. Indeed, the expected outcome manifested as the number of joint evaluations per data point grows with a scaling exponent slightly above one for CIFAR-10, CelebA, and SVHN, indicating that em-MFA scales slightly superlinearly with C , due to a slightly increasing number of iterations until convergence with more components. Conversely, for EMNIST, the exponent falls slightly below one, due to a slight decrease in the number of iterations for em-MFA (as well as v-MFA) on this dataset.

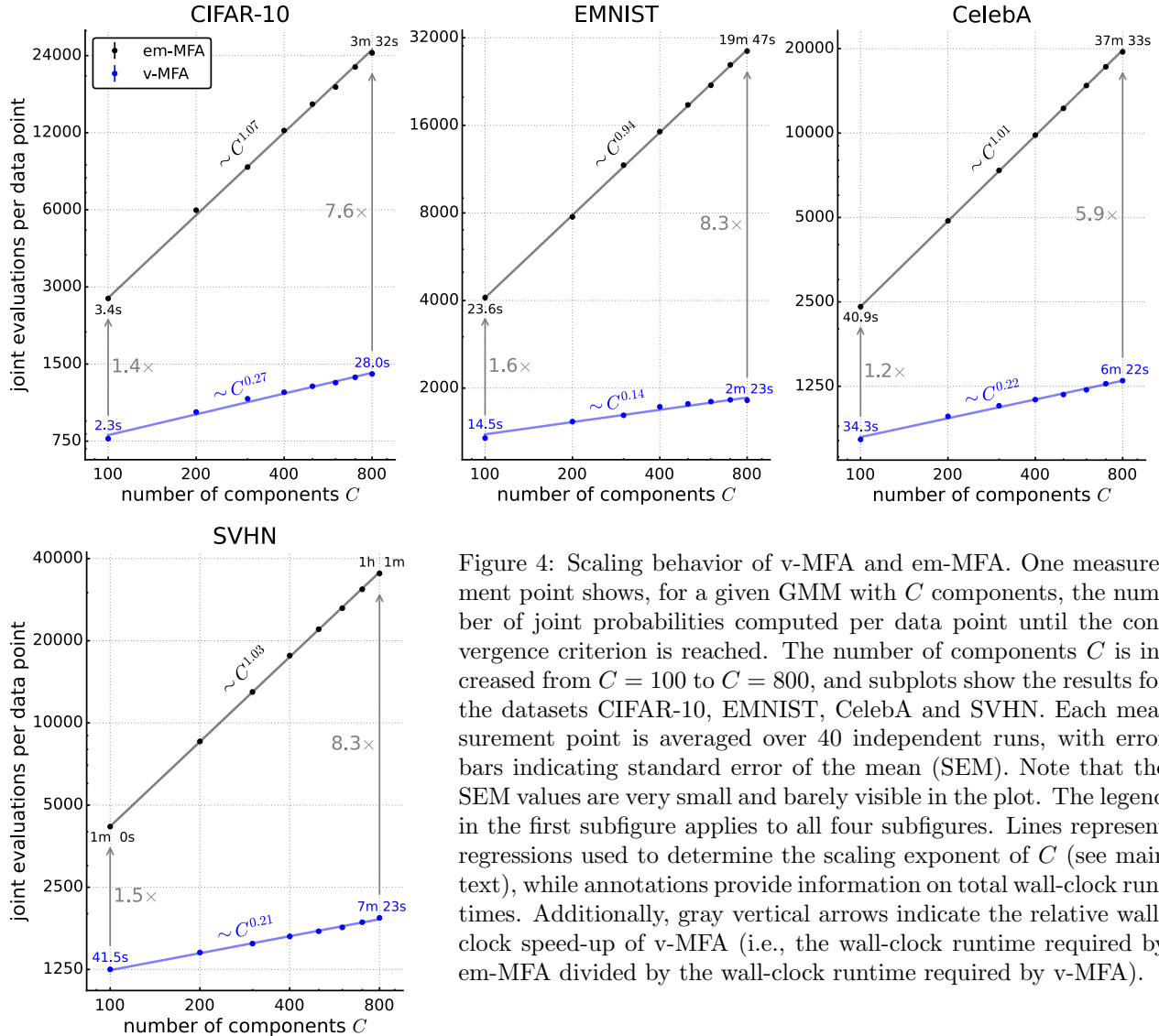


Figure 4: Scaling behavior of v-MFA and em-MFA. One measurement point shows, for a given GMM with C components, the number of joint probabilities computed per data point until the convergence criterion is reached. The number of components C is increased from $C = 100$ to $C = 800$, and subplots show the results for the datasets CIFAR-10, EMNIST, CelebA and SVHN. Each measurement point is averaged over 40 independent runs, with error bars indicating standard error of the mean (SEM). Note that the SEM values are very small and barely visible in the plot. The legend in the first subfigure applies to all four subfigures. Lines represent regressions used to determine the scaling exponent of C (see main text), while annotations provide information on total wall-clock runtimes. Additionally, gray vertical arrows indicate the relative wall-clock speed-up of v-MFA (i.e., the wall-clock runtime required by em-MFA divided by the wall-clock runtime required by v-MFA).

In contrast to em-MFA, the number of joint evaluations per data point is in each iteration upper-bounded for v-MFA. Concretely, the number of joint evaluations for v-MFA is bounded by the size of all search spaces $\mathcal{S}^{(n)}$, which remains constant relative to C . In practice, the actual number tends to be lower than this bound due to intersections of the sets g_c . However, v-MFA typically requires more iterations than em-MFA due to its partial E-steps (and its additional initial partial E-steps). In principle, a larger number of iterations until convergence could result in v-MFA being less efficient than em-MFA across the whole optimization procedure. Considering Fig. 4, however, our numerical evaluation clearly shows a significant gain in computational efficiency. Importantly, the efficiency gain presents itself as a different scaling of the computational complexity with C (in contrast to, e.g., a constant offset). Concretely, we observed for all datasets that the number of joint evaluations per data point scales sublinearly with C , with all scaling exponents consistently below $1/3$ (which corresponds to a cubic root dependency, $\sqrt[3]{C}$). For instance, when considering $C = 100$, the required number of joint evaluations for em-MFA was approximately three times higher compared to v-MFA across all datasets. However, as C increased to the highest examined value of $C = 800$, the difference in the number

of joint evaluations spanned an order of magnitude. For even larger C , the reduction in joint evaluations for v-MFA compared to em-MFA still increases further (we investigate such larger C in the next sections).

When observing the training time (depicted as annotations in Fig. 4), we discerned marginal speed-ups of v-MFA compared to em-MFA already for $C = 100$. For $C = 800$, the training speed of v-MFA then substantially surpassed that of em-MFA, highlighting the practical effectiveness of the novel approach not solely in terms of theoretical complexity scaling but also in terms of concrete runtime reductions. Analogous to the reduction of joint evaluations, the improvements in runtimes are expected to increase further with larger values of C (cf. Sec. 3.3).

We note that the results reported in Fig. 4 are solely instructive about the computational cost of the algorithms until convergence. The results are not calibrated w.r.t. quality of the optimization results. To ensure that the observed improvements of v-MFA in computational complexity are not primarily due to a loss in quality, additional control experiments were conducted (see Appendix B.2.3). Indeed, a slight loss in optimization quality can be observed for v-MFA compared to em-MFA. However, the loss is small and if we compare the computational complexity of v-MFA and em-MFA required to achieve the same optimization quality (in terms of NLL_{test}), the sublinear speed-up of v-MFA compared to em-MFA remains essentially the same as in Fig. 4. Only for EMNIST (which showed one of the strongest speed-ups of v-MFA compared to em-MFA) a non-negligible (but still small) fraction of the speed-up is due to a reduction in quality. Optimization times, optimization qualities and their interdependence are investigated more systematically in the next section (Sec. 3.2).

3.2 Quality vs. Efficiency Analysis

In the experiments detailed in Sec. 3.1, it was shown that the number of joint evaluations per data point exhibits sublinear scaling w.r.t. the number of components C for the v-MFA algorithm. While the complexity scaling with C was our main interest in the previous experiments, in this subsection we systematically compare the optimization quality and efficiency. Therefore, we measured optimization quality and efficiency using different algorithms applied to the four datasets of Tab. 1. We compared algorithms, including em-MFA and v-MFA, across different settings in terms of wall-clock runtimes vs. optimization quality, with quality measured in terms of the relative NLL values on the testsets.

If only those NLL values of the algorithms v-MFA and em-MFA were presented, the differences in their values may lack a meaningful reference. Therefore, we also included NLL values of the parameters after initialization, illustrating the learning improvements of the algorithms. Furthermore, we compared v-MFA and em-MFA to the k -means+FA algorithm, which combines k -means with factor analyzers (for details on the algorithm, see Appendix B.1.1). With this methodology, we followed [18], who combined k -means and factor analysis as an initialization procedure for MFA optimization.

For each of the four datasets, we selected a different number of components, with $C = 800, 1200, 1800$, and 2000 for CIFAR-10, CelebA, SVHN and EMNIST, respectively. The number of latent dimensions is held constant at $H = 5$ across all datasets. Additionally, for the v-MFA algorithm, we measured the performance across nine different settings of the hyperparameters C' and G (all combinations of $C' \in \{3, 5, 7\}$ and $G \in \{5, 15, 30\}$). We initialized the parameters of v-MFA, em-MFA and k -means+FA (means only) identically, following the procedures outlined in Sec. 2.4. Fig. 5 shows the NLL_{test} values relative to em-MFA for the different algorithms (and different settings for v-MFA) against their wall-clock runtimes.

In general, all algorithms significantly improved the NLL compared to the initial NLL values. The em-MFA algorithm achieved the best (lowest) NLL values on the EMNIST and SVHN datasets, while the v-MFA algorithm performed best on the CIFAR-10 and CelebA datasets (with $C' = 3$ and $G = 5$). The relative deviations of v-MFA from the baseline remained consistently below 0.32%, with most settings of the hyperparameters C' and G showing even smaller deviations. The k -means+FA algorithm showed significantly

higher NLL values, exhibiting a deviation from baseline by approximately 1% for datasets such as CelebA and CIFAR-10, and up to 3% and 7% for the SVHN and EMNIST datasets, respectively.

In terms of runtime, the v-MFA algorithm (with $C' = 3$ and $G = 5$) was the fastest among the algorithms evaluated on all four datasets (excluding Initialization). Across all settings of hyperparameters C' and G , v-MFA consistently outperformed em-MFA, achieving significant speed-ups ranging from $3.3\times$ to $25.6\times$. Additionally, v-MFA achieved faster runtimes than k -means+FA for the majority of hyperparameter settings.

Further details on the results of these experiments are provided in Appendix B.3. Additionally, we present in Appendix B.2.2 control experiments for v-MFA, em-MFA and k -means+FA compared to previously studied large-scale MFA optimization [18] based on stochastic gradient descent (SGD).

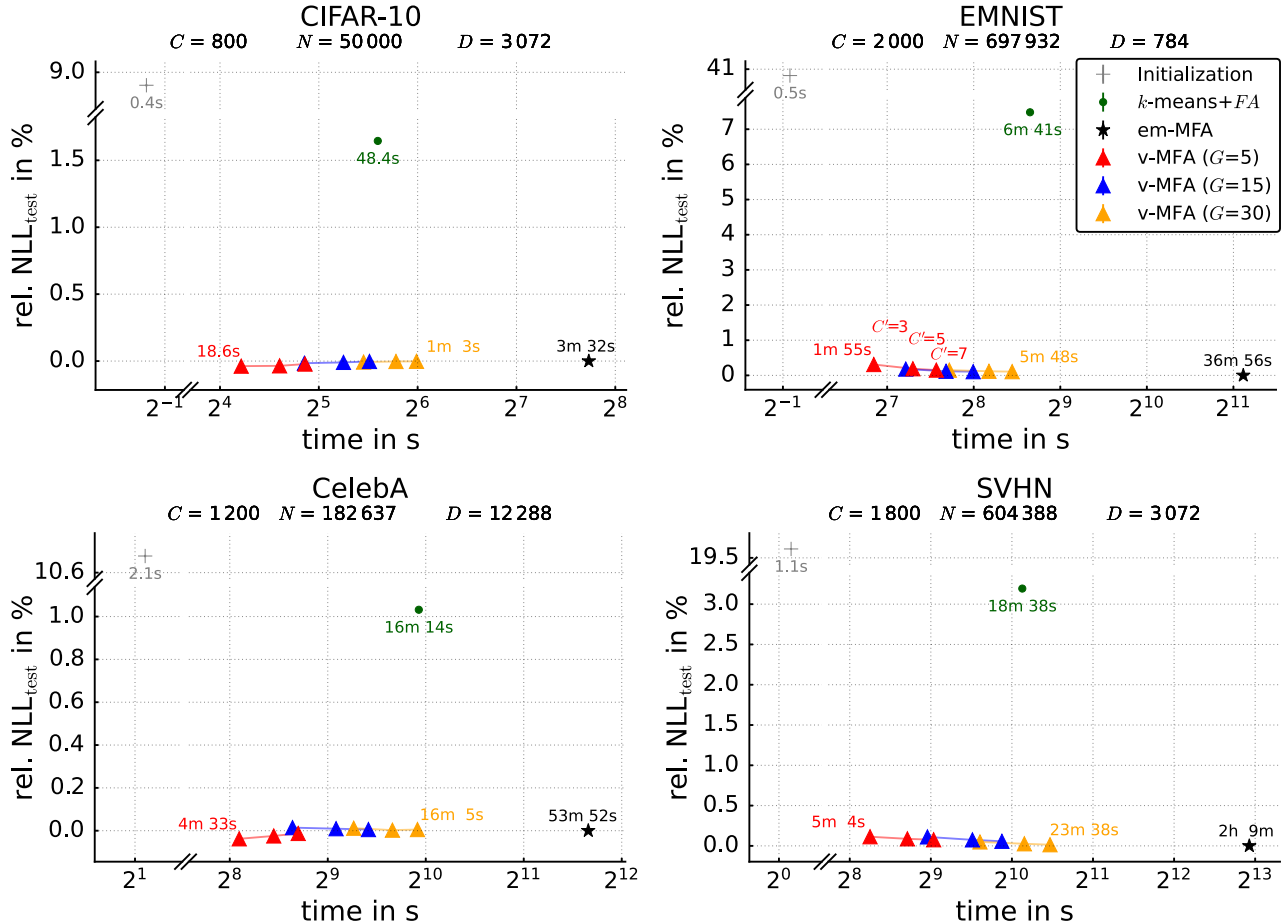


Figure 5: Effectiveness and efficiency in terms of negative log-likelihood (NLL) and runtime of v-MFA compared to em-MFA, k -means+FA and the parameters after initialization. Each of the four subfigures refers to experiments on one benchmark dataset. The y-axes denote the relative NLL on the testset w.r.t. em-MFA as baseline, given by Eq. (16). For the v-MFA algorithm, we present the performance across nine different settings of the hyperparameters C' and G . For each configuration of $G \in \{5, 15, 30\}$, measurements for the v-MFA algorithm (three red, blue and yellow triangles, respectively) refer to configurations with $C' \in \{3, 5, 7\}$. Settings with larger C' lie to the right, as they required longer runtimes. Each measurement point is averaged over 40 independent runs, with error bars indicating standard error of the mean (SEM) (note that the SEM values are smaller than the symbol sizes).

3.3 GMMs with up to Billions of Parameters

All numerical investigations in Secs. 3.1 and 3.2 conducted so far have allowed for the application of em-MFA (or k -means+FA). However, the sublinear scaling provided by v-MFA does allow for addressing much larger scale problems. For this section, we therefore investigated such significantly larger scale problems, which far exceed the problem sizes that can be addressed by em-MFA or other GMM approaches (on current, reasonable compute resources). Concretely, we used a dataset with approximately 100M images, each of size $D = 32 \times 32 \times 3 = 3072$, and applied the v-MFA algorithm using up to $C = 500\,000$ components. The used dataset is a version of the YFCC100M dataset (see Appendix B.1.3 for details), of which we randomly selected 5% of the samples as a testset and used the remaining 95% for training (see Tab. 2).

Table 2: Specifications of the YFCC100M dataset. The data dimension is given in pixel width \times pixel height \times color channels.

dataset	train samples	test samples	data dimension D
YFCC100M [45]	94 197 533	4 957 765	$32 \times 32 \times 3 = 3072$

For our series of experiments, we used $C = 500, 5000, 50\,000$ and $500\,000$ as the number of components of the MFA model. Unlike in Sec. 3.1, we always trained the algorithm using all training samples (regardless of the chosen value of C). For the other hyperparameters, we adopted the same settings as in Sec. 3.1, namely $H = 5, C' = 3$ and $G = 15$. The total number of trainable MFA parameters is given by $C(D(H + 2) + 1) - 1$. Consequently, when using $C = 500\,000$ and $H = 5$, the MFA model comprises more than 10^{10} (i.e., more than ten billion) parameters that are optimized by the v-MFA algorithm on the given dataset.

Due to the computational complexity of AFK-MC², which scales quadratically with C , this type of initialization becomes prohibitively demanding for larger values of C used in these experiments. Therefore, we used a less sophisticated initialization method. For the initial $\mu_{1:C}$, we selected data points uniformly at random (avoiding duplicates). Diagonal variances and factor loadings were initialized as previously described. To further mitigate the cost of initialization, the convergence threshold for *warm-up* was set to 10^{-3} , i.e., to a larger value than for the previous smaller scale experiments (see Sec. 2.4).

During our experiments with $C = 50\,000$ and $500\,000$, we observed that due to the less sophisticated initialization some components became excluded from all $\mathcal{K}^{(n)}$ in the training process, resulting in "empty" components. These empty components were not further considered, effectively reducing C . But the number of empty components was less than 0.2% of C in all experiments.

Fig. 6 shows the measured computational costs and NLL values for the conducted series of very large scale MFA optimizations. In Fig. 6A, the main observation is that both the number of joint evaluations and the training runtime increased only moderately as C increased. This behavior is a direct consequence of the sublinear scaling of v-MFA. From $C = 50\,000$ to $C = 500\,000$, runtimes even slightly decreased, which is due to a slight reduction in the number of iterations.

At the same time, increasing the size of the MFA model by increasing the number of components C resulted in a substantial decrease in the NLL on the testset (Fig. 6B). For $C = 500$, the NLL values for em-MFA and v-MFA were statistically equivalent within the standard error of the mean. This finding aligns with the observations in Sec. 3.2, where only minor differences in NLL values were reported between the two algorithms. Scaling em-MFA to component numbers significantly larger than $C = 500$ was computationally prohibitive. Already for $C = 500$, em-MFA required approximately two days to train compared to approximately 5 hours for v-MFA and em-MFA required on average $16.6\times$ as many joint evaluations. For $C = 5000$ the runtime of em-MFA would be significantly slower (by about an order of magnitude). Additionally, Fig. 6A shows that v-MFA requires even fewer joint evaluations for the whole optimization procedure than em-MFA does for a

single iteration.

Our largest scale experiments for v-MFA (with $C = 500\,000$) finally demonstrate that with current hardware³, an MFA model with more than 10 billion parameters can be optimized in less than nine hours.

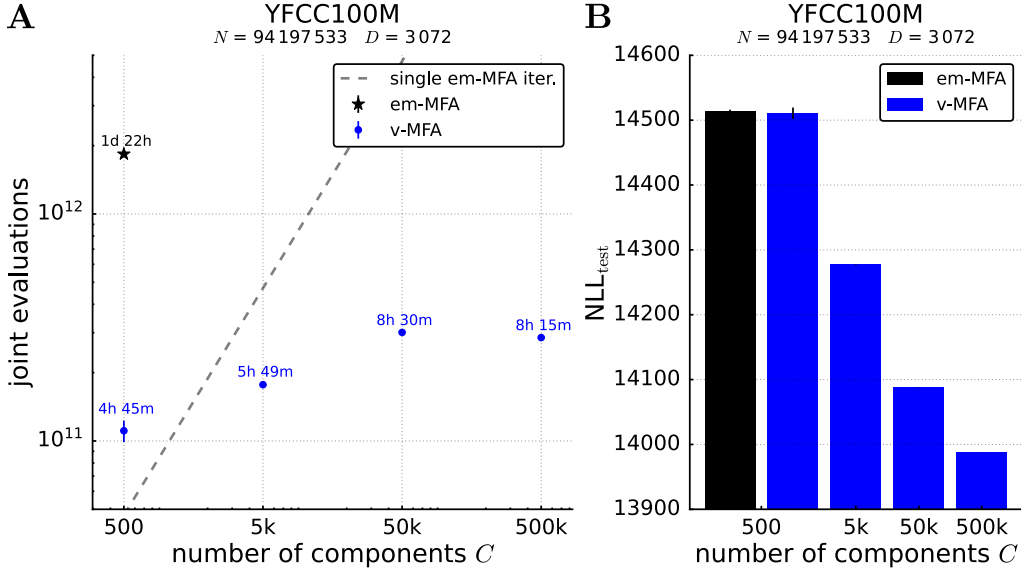


Figure 6: Evaluation of v-MFA and em-MFA on the YFCC100M dataset. In **A**, the total numbers of joint evaluations until convergence for different C values are illustrated. Annotations provide insight into the total training time. Additionally, the dashed gray line represents the number of joint evaluations for a single iteration of em-MFA (theoretically given by NC). In **B**, the values of the negative log-likelihood per data point on the testset for em-MFA with $C = 500$ and for v-MFA with different number of components C are shown. In both figures, each measurement point is averaged over 3 independent runs and error bars denote the standard error of the mean (SEM).

4 Discussion

A salient hallmark of GMMs (in contrast, e.g., to k -means) is their flexible parametrization of data correlations within components. Furthermore, intra-component correlations and large numbers of components C allow GMMs to approximate potentially intricate data density with increasing accuracy as C grows [e.g. 6–8]. However, this flexibility comes at a substantial cost, namely a very high computational demand for the optimization of general GMMs with large C .

In this contribution, we have addressed the problem of high optimization costs for GMMs with flexible covariances. Such flexible GMMs have not been addressed by previous approaches that used related variational approaches [12, 13, 46].

Notably, the here derived algorithm, v-MFA, does not reduce runtimes by a fixed constant amount or percentage but (more substantially) shows another scaling of runtime complexity: as the number of data points N and components C increase, the runtime per iteration scales *sublinearly* with NC . Achieving such a sublinear scaling for MFA optimization was the main goal of the research here reported.

³We used a node with considerable compute resources, i.e., v-MFA was trained utilizing all 64 cores of a single AMD Genoa EPYC 9554 CPU and 4 TB of RAM.

The optimized MFA models still remain elementary data models. In comparison to general GMMs, they can be regarded as assuming the data to lie close to low-dimensional manifolds, which are approximated piecewise by low-dimensional hyperplanes. Otherwise, no additional assumptions or structures are imposed beyond the standard assumptions of GMMs. Consequently, applications of the v-MFA algorithm to tasks previously addressed using GMMs should not be expected to show improvements in quality if GMMs or MFAs of the same size are used. However, for applications involving large GMMs, the v-MFA algorithm provides a much more efficient optimization algorithm. Except for the submanifold assumption, the optimized MFA models used by v-MFA retain the flexibility of GMMs in terms of within-component correlations. When the data dimensionality D is not too high, full GMMs (i.e., GMMs with full covariance matrices) can also be optimized using the proposed approach. Our numerical analyses show that the optimization quality achieved by v-MFA is very similar to the optimization quality of conventional GMM or MFA optimization. The key advantage of v-MFA is, however, its significantly faster optimization times — potentially an order of magnitude or more faster than conventional training (see Secs. 3.1 and 3.2). For very large scales, v-MFA is therefore likely to be the only applicable approach (see Sec. 3.3). To the authors’ best knowledge, v-MFA is currently the only approach allowing for the optimization of flexible GMMs with billions of parameters. As an outlook, v-MFA enables the investigation of GMMs at scales typically reserved for other classes of machine learning models, such as deep probabilistic models. The largest-scale such models exclusively trained on image data are reported in the recent literature to range from hundreds of millions to about one billion parameters [47–49] (also compare [50, 51] for other domains). Given that GMMs are universal density approximators, the novel ability to optimize GMMs with billions of parameters (as discussed in Sec. 3.3) positions such giant GMMs as potentially valuable tools for large-scale machine learning. The here established scalability is particularly relevant in the context of large datasets and models, which are currently central in driving the whole field of artificial intelligence.

5 Conclusion

We introduced a highly efficient optimization algorithm for as flexible as possible Gaussian Mixture Models (GMMs). Concretely, we combined a mixture of factor analyzers (MFA) as GMM approximation (compare [18, 30, 31]) with a novel and highly efficient variational optimization method derived in this work to optimize MFA parameters. The central part of the optimization are variational E-steps (Secs. 2.1 to 2.3) which effectively optimize variational parameters. For each E-step we ensured that its computational complexity per data point is by definition constant w.r.t. C (no linear scaling with C , cf. Alg. 3). We then empirically showed (Sec. 3.1) that the complexity reduction per iteration translates to a sublinear scaling of the whole optimization procedure. In systematic investigations of the whole MFA optimization process, we observed scalings with C below cubic roots of C (see Fig. 4 for details). Furthermore, the observed scaling behavior led to significantly shorter wall-clock runtimes on standard benchmarks (Sec. 3.2). The here reported sublinear runtime scaling of GMM optimization represents our main contribution. As an example exploiting sublinear scaling, we demonstrated that the v-MFA algorithm can optimize GMMs at scales that could previously not be addressed. Concretely, using approximately 100 million images, we reported (in Sec. 3.3) results for a GMM model with more than 10 billion parameters that was optimized by v-MFA on a single compute node in less than nine hours.

The optimization of MFAs by the v-MFA algorithm can not be expected to improve the optimization quality compared to conventional GMM or MFA optimization methods. On the contrary, for the same MFA model, a decrease in optimization quality has to be anticipated as the applied variational approach is an approximation of conventional MFA optimization. However, in our experiments, the effect on optimization quality was small, i.e., we either observed no or only a marginal reduction in quality (see Secs. 3.2 and 3.3) when applying the v-MFA algorithm instead of conventional EM optimization.

Importantly, the v-MFA algorithm enables the application of GMMs to large-scale tasks that were previously

considered unsuitable or impractical for GMMs due to the high computational cost of conventional optimization. Future research could explore the application of v-MFA to such large-scale tasks. Another potential direction for future research is to extend the proposed variational optimization algorithm to other types of mixture models [52].

Acknowledgements

We thank Jan Warnken, Roy Friedman and Yair Weiss for valuable discussions and feedback.

References

- [1] McLachlan, G. & Peel, D. *Finite Mixture Models* (Wiley, 2000).
- [2] Bishop, C. M. *Pattern Recognition and Machine Learning* (Springer, 2006).
- [3] Bouguila, N. & Fan, W. (eds.) *Mixture Models and Applications* (Springer, 2020).
- [4] Zoran, D. & Weiss, Y. From learning models of natural image patches to whole image restoration. In *2011 International Conference on Computer Vision*, 479–486 (IEEE, 2011).
- [5] Tian, T., Wan, J., Song, Q. & Wei, Z. Clustering single-cell RNA-seq data with a model-based deep learning approach. *Nature Machine Intelligence* **1**, 191–198 (2019).
- [6] Zeevi, A. J. & Meir, R. Density estimation through convex combinations of densities: approximation and estimation bounds. *Neural Networks* **10**, 99–109 (1997).
- [7] Li, J. Q. & Barron, A. R. Mixture density estimation. In *Proceedings of the 12th International Conference on Neural Information Processing Systems*, 279–285 (MIT Press, 1999).
- [8] Maz'ya, V. & Schmidt, G. On approximate approximations using Gaussian kernels. *IMA Journal of Numerical Analysis* **16**, 13–29 (1996).
- [9] Parzen, E. On estimation of a probability density function and mode. *The Annals of Mathematical Statistics* **33**, 1065–1076 (1962).
- [10] Dempster, A. P., Laird, N. M. & Rubin, D. B. Maximum Likelihood from Incomplete Data via the EM Algorithm (with discussion). *Journal of the Royal Statistical Society B* **39**, 1–38 (1977).
- [11] Asheri, H., Hosseini, R. & Araabi, B. N. A new EM algorithm for flexibly tied GMMs with large number of components. *Pattern Recognition* **114**, 107836 (2021).
- [12] Hirschberger, F., Forster, D. & Lücke, J. A Variational EM Acceleration for Efficient Clustering at Very Large Scales. *IEEE Transactions on Pattern Analysis and Machine Intelligence* **44**, 9787–9801 (2022).
- [13] Exarchakis, G., Oubari, O. & Lenz, G. A Sampling-Based Approach for Efficient Clustering in Large Datasets. In *Proceedings of the IEEE/CVF Conference on Computer Vision and Pattern Recognition*, 12403–12412 (2022).
- [14] Elkan, C. Using the triangle inequality to accelerate k-means. In *Proceedings of the 20th International Conference on International Conference on Machine Learning*, 147–153 (AAAI Press, 2003).
- [15] Cheng, D.-Y., Gersho, A., Ramamurthi, B. & Shoham, Y. Fast search algorithms for vector quantization and pattern matching. In *IEEE International Conference on Acoustics, Speech, and Signal Processing*, vol. 9, 372–375 (1984).

- [16] Bei, C.-D. & Gray, R. An improvement of the minimum distortion encoding algorithm for vector quantization. *IEEE Transactions on Communications* **33**, 1132–1133 (1985).
- [17] Chan, J. Y. K. & Leung, A. P. Efficient k-means++ with random projection. In *2017 International Joint Conference on Neural Networks*, 94–100 (2017).
- [18] Richardson, E. & Weiss, Y. On GANs and GMMs. In *Proceedings of the 32nd International Conference on Neural Information Processing Systems*, 5852–5863 (Curran Associates Inc., 2018).
- [19] Hertrich, J. *et al.* PCA reduced Gaussian mixture models with applications in superresolution. *Inverse Problems and Imaging* **16**, 341–366 (2022).
- [20] Liu, Z., Yu, L., Hsiao, J. H. & Chan, A. B. PRIMAL-GMM: PaRAMetric MANifold Learning of Gaussian Mixture Models. *IEEE Transactions on Pattern Analysis and Machine Intelligence* **44**, 3197–3211 (2022).
- [21] Bouveyron, C., Girard, S. & Schmid, C. High-dimensional data clustering. *Computational Statistics & Data Analysis* **52**, 502–519 (2007).
- [22] Lucic, M., Faulkner, M., Krause, A. & Feldman, D. Training Gaussian Mixture Models at Scale via Coresets. *Journal of Machine Learning Research* **18**, 1–25 (2018).
- [23] Har-Peled, S. & Mazumdar, S. On coresets for k-means and k-median clustering. In *Proceedings of the Thirty-Sixth Annual ACM Symposium on Theory of Computing*, 291–300 (ACM, 2004).
- [24] Feldman, D., Faulkner, M. & Krause, A. Scalable training of mixture models via coresets. In *Advances in Neural Information Processing Systems*, vol. 24, 2142–2150 (Curran Associates, Inc., 2011).
- [25] Nguyen, H. D., Forbes, F. & McLachlan, G. J. Mini-batch learning of exponential family finite mixture models. *Statistics and Computing* **30**, 731–748 (2020).
- [26] Sculley, D. Web-scale k-means clustering. In *Proceedings of the 19th International Conference on World Wide Web*, 1177–1178 (ACM, 2010).
- [27] Liu, J. *et al.* Large-Scale Clustering on 100M-Scale Datasets Using a Single T4 GPU via Recall KNN and Subgraph Segmentation. *Neural Processing Letters* **56** (2024).
- [28] Lücke, J. & Eggert, J. Expectation Truncation And the Benefits of Preselection in Training Generative Models. *Journal of Machine Learning Research* **11**, 2855–2900 (2010).
- [29] Drefs, J., Guiraud, E. & Lücke, J. Evolutionary Variational Optimization of Generative Models. *Journal of Machine Learning Research* **23**, 1–51 (2022).
- [30] Ghahramani, Z. & Hinton, G. E. The EM algorithm for mixtures of factor analyzers. Technical Report CRG-TR-96-1, University of Toronto (1996).
- [31] McLachlan, G., Peel, D. & Bean, R. Modelling high-dimensional data by mixtures of factor analyzers. *Computational Statistics & Data Analysis* **41**, 379–388 (2003).
- [32] Arthur, D. & Vassilvitskii, S. k-means++: the advantages of careful seeding. In *Proceedings of the 18th Annual ACM-SIAM Symposium on Discrete Algorithms*, 1027–1035 (SIAM, 2007).
- [33] Bachem, O., Lucic, M., Hassani, S. H. & Krause, A. Approximate K-Means++ in Sublinear Time. In *Proceedings AAAI Conference on Artificial Intelligence*, vol. 30, 1459–1467 (2016).
- [34] Bachem, O., Lucic, M., Hassani, H. & Krause, A. Fast and Provably Good Seedings for k-means. In *Advances in Neural Information Processing Systems*, vol. 29, 55–63 (Curran Associates, Inc., 2016).

- [35] Fränti, P. & Sieranoja, S. How much can k-means be improved by using better initialization and repeats? *Pattern Recognition* **93**, 95–112 (2019).
- [36] Neal, R. & Hinton, G. A View of the EM Algorithm that Justifies Incremental, Sparse, and other Variants. *Learning in Graphical Models* 355–368 (1998).
- [37] Jordan, M. I., Ghahramani, Z., Jaakkola, T. S. & Saul, L. K. An Introduction to Variational Methods for Graphical Models. *Machine Learning* **37**, 183–233 (1999).
- [38] Shelton, J. A., Gasthaus, J., Dai, Z., Lücke, J. & Gretton, A. GP-select: Accelerating EM using adaptive subspace preselection. *Neural Computation* **29**, 2177–2202 (2017).
- [39] Forster, D., Sheikh, A.-S. & Lücke, J. Neural Simpletrons: Learning in the Limit of Few Labels with Directed Generative Networks. *Neural Computation* **30**, 2113–2174 (2018).
- [40] Lücke, J. Truncated Variational Expectation Maximization. *arXiv:1610.03113v3* (2019).
- [41] Krizhevsky, A. Learning multiple layers of features from tiny images (2009).
- [42] Liu, Z., Luo, P., Wang, X. & Tang, X. Deep Learning Face Attributes in the Wild. In *Proceedings of the IEEE International Conference on Computer Vision*, 3730–3738 (2015).
- [43] Cohen, G., Afshar, S., Tapson, J. & van Schaik, A. EMNIST: Extending MNIST to handwritten letters. In *2017 International Joint Conference on Neural Networks*, 2921–2926 (IEEE, 2017).
- [44] Netzer, Y. *et al.* Reading Digits in Natural Images with Unsupervised Feature Learning. In *NeurIPS Workshop on Deep Learning and Unsupervised Feature Learning 2011* (2011).
- [45] Thomee, B. *et al.* YFCC100M: The new data in multimedia research. *Communications of the ACM* **59**, 64–73 (2016).
- [46] Lücke, J. & Forster, D. k-means as a variational EM approximation of Gaussian mixture models. *Pattern Recognition Letters* **125**, 349–356 (2019).
- [47] Dosovitskiy, A. *et al.* An Image is Worth 16x16 Words: Transformers for Image Recognition at Scale. In *International Conference on Learning Representations* (2021).
- [48] Fang, Y. *et al.* EVA: Exploring the Limits of Masked Visual Representation Learning at Scale. In *Proceedings of the IEEE/CVF Conference on Computer Vision and Pattern Recognition*, 19358–19369 (2023).
- [49] Wortsman, M. *et al.* Stable and low-precision training for large-scale vision-language models. In *Proceedings of the 37th International Conference on Neural Information Processing Systems*, 10271 – 10298 (Curran Associates Inc., 2024).
- [50] Hsu, W.-N. *et al.* HuBERT: Self-Supervised Speech Representation Learning by Masked Prediction of Hidden Units. *IEEE/ACM Transactions on Audio, Speech, and Language Processing* **29**, 3451–3460 (2021).
- [51] Frey, N. C. *et al.* Neural scaling of deep chemical models. *Nature Machine Intelligence* **5**, 1297–1305 (2023).
- [52] Banerjee, A., Merugu, S., Dhillon, I. S., Ghosh, J. & Lafferty, J. Clustering with Bregman Divergences. *Journal of Machine Learning Research* **6**, 1705–1749 (2005).

- [53] Zhao, J.-H. & Yu, P. L. H. Fast ML Estimation for the Mixture of Factor Analyzers via an ECM Algorithm. *IEEE Transactions on Neural Networks* **19**, 1956–1961 (2008).
- [54] Blum, M., Floyd, R. W., Pratt, V., Rivest, R. L. & Tarjan, R. E. Time bounds for selection. *Journal of Computer and System Sciences* **7**, 448–461 (1973).
- [55] Guennebaud, G., Jacob, B. *et al.* Eigen v3. <http://eigen.tuxfamily.org> (2010).
- [56] The Boost organization. Boost C++ Libraries. <http://www.boost.org> (2024).
- [57] Jakob, W., Rhinelander, J. & Moldovan, D. pybind11 – Seamless operability between C++11 and Python. <https://github.com/pybind/pybind11> (2017).
- [58] Ansel, J. *et al.* PyTorch 2: Faster Machine Learning Through Dynamic Python Bytecode Transformation and Graph Compilation. In *29th ACM International Conference on Architectural Support for Programming Languages and Operating Systems*, vol. 2 (ACM, 2024).
- [59] Pedregosa, F. *et al.* Scikit-learn: Machine Learning in Python. *Journal of Machine Learning Research* **12**, 2825–2830 (2011).
- [60] Richardson, E. torch-mfa. *GitHub Repository*. <https://github.com/eitanrich/torch-mfa> (2019).
- [61] Tange, O. GNU Parallel 20210822 ('Kabul') (2021).

Appendix

A Supporting Information on Materials and Methods

In the following, we provide further details on techniques to avoid inversions of large covariance matrices in Appendix A.1, the derivation of the M-step parameter updates in Appendix A.2, the proof of Proposition 1 in Appendix A.3, additional information on the estimation of component-to-component distances and the KL-divergence in Appendix A.4, as well as further details on the algorithmic complexity of the variational E-step in Appendix A.5.

A.1 Avoiding Inversion of Large Covariance Matrices in MFAs

Optimizing the MFA model using EM or variational EM requires to repeatedly evaluate joint probabilities $p(c, \mathbf{x}_n | \Theta)$ or, equivalently, log-joints. Thus, it is essential to assess the efficiency of log-joint evaluations. Given that

$$\begin{aligned} \log p(\mathbf{x}_n, c | \Theta) &= \log p(c | \Theta) + \log p(\mathbf{x}_n | c, \Theta) \\ &= \log \pi_c - \frac{D}{2} \log(2\pi) - \frac{1}{2} \log |\Sigma_c| - \frac{1}{2} (\mathbf{x}_n - \boldsymbol{\mu}_c)^\top \Sigma_c^{-1} (\mathbf{x}_n - \boldsymbol{\mu}_c), \end{aligned} \quad (\text{A1})$$

the crucial aspects include the evaluation of the Mahalanobis distance $(\mathbf{x}_n - \boldsymbol{\mu}_c)^\top \Sigma_c^{-1} (\mathbf{x}_n - \boldsymbol{\mu}_c)$, which necessitates inverting Σ_c , and the determinant computation for $\log |\Sigma_c|$. Direct calculations involving Σ_c become computationally expensive for high-dimensional data. To enhance computational efficiency, we adopt methods from [18, 30, 31]. Specifically, for the inversion of Σ_c , we utilize Woodbury’s matrix inversion lemma

$$\Sigma_c^{-1} = \mathbf{D}_c^{-1} - \mathbf{D}_c^{-1} \Lambda_c \left(\mathbf{I} + \Lambda_c^\top \mathbf{D}_c^{-1} \Lambda_c \right)^{-1} \Lambda_c^\top \mathbf{D}_c^{-1} = \mathbf{D}_c^{-1} - \mathbf{U}_c \mathbf{V}_c \quad (\text{A2})$$

where we define

$$\mathbf{U}_c := \mathbf{D}_c^{-1} \Lambda_c \in \mathbb{R}^{D \times H}, \quad \mathbf{L}_c := \mathbf{I} + \Lambda_c^\top \mathbf{D}_c^{-1} \Lambda_c = \mathbf{I} + \mathbf{U}_c^\top \Lambda_c \in \mathbb{R}^{H \times H}, \quad (\text{A3})$$

$$\mathbf{V}_c := \mathbf{L}_c^{-1} \Lambda_c^\top \mathbf{D}_c^{-1} = \mathbf{L}_c^{-1} \mathbf{U}_c^\top \in \mathbb{R}^{H \times D}. \quad (\text{A4})$$

Given that \mathbf{D}_c is diagonal, its inversion is trivial. Furthermore, the inversion of the matrix \mathbf{L}_c is of size $H \times H$ and can therefore be inverted more efficiently than the $D \times D$ covariance matrix (especially for $H \ll D$). As a quantification of complexity, it is evident from Eq. (A2) that the Mahalanobis distance, expressed as

$$\mathbf{v}^\top \Sigma_c^{-1} \mathbf{v} = \mathbf{v}^\top \mathbf{D}_c^{-1} \mathbf{v} - (\mathbf{v}^\top \mathbf{U}_c) (\mathbf{V}_c \mathbf{v}), \quad (\text{A5})$$

can be evaluated with complexity $\mathcal{O}(DH)$ for any $\mathbf{v} \in \mathbb{R}^D$.

Finally, log-determinant is obtained using the matrix determinant lemma

$$\log |\Sigma_c| = \log \left| \Lambda_c \Lambda_c^\top + \mathbf{D}_c \right| = \log \left| \mathbf{I} + \Lambda_c^\top \mathbf{D}_c^{-1} \Lambda_c \right| + \log |\mathbf{D}_c| = \log |\mathbf{L}_c| + \sum_d \log \sigma_{cd}^2.$$

In conclusion, we can efficiently compute the log-joints for high-dimensional data such as images, circumventing direct computations involving covariance matrices of size $D \times D$.

The derivation for the parameter updates in the M-step that maintain efficiency for high D is provided in Appendix A.2. Although there exist alternative optimization methods to EM, such as Alternating Expectation Conditional Maximization (AECM) [31] and Expectation Conditional Maximization (ECM) [53], we keep in line with the EM approach. AECM requires two cycles, involving two E-steps to update all model parameters, and the conditional M-step updates in AECM and ECM lead to higher computational complexities in D or H .

A.2 Derivation of the M-step Parameter Updates

In this section, we derive the parameter updates for the M-step of the MFA model, specified in Eq. (1) in the main text, following the derivations outlined in [30]. Since our parameter updates deviate from [30] in certain aspects, e.g., using a variational approach with truncated posteriors or individual diagonal variances \mathbf{D}_c for each component, we present here the complete derivations for clarity and completeness.

In the following, we always denote the variational parameters $\tilde{\Theta}$ with a tilde, e.g., $\tilde{\boldsymbol{\mu}}_c$, where $\boldsymbol{\mu}_c$ (without a tilde) corresponds to the model parameters Θ . Recall that the MFA generative model is given by

$$p(c | \Theta) = \pi_c, \quad p(\mathbf{z} | \Theta) = \mathcal{N}(\mathbf{z}; \mathbf{0}, \mathbf{I}), \quad p(\mathbf{x} | \mathbf{z}, c, \Theta) = \mathcal{N}(\mathbf{x}; \boldsymbol{\Lambda}_c \mathbf{z} + \boldsymbol{\mu}_c, \mathbf{D}_c). \quad (\text{A6})$$

We start here by introducing truncated posteriors as variational distributions given by

$$\begin{aligned} q(c, \mathbf{z}; \mathbf{x}_n, \mathcal{K}^{(n)}, \tilde{\Theta}) &= \frac{1}{Z_n} p(c, \mathbf{z} | \mathbf{x}_n, \tilde{\Theta}) \delta(c \in \mathcal{K}^{(n)}) \\ &= \frac{1}{Z_n} p(c | \mathbf{x}_n, \tilde{\Theta}) p(\mathbf{z} | c, \mathbf{x}_n, \tilde{\Theta}) \delta(c \in \mathcal{K}^{(n)}) \\ &= q_n(c | \tilde{\Theta}) q_{n,c}(\mathbf{z} | \tilde{\Theta}), \end{aligned} \quad (\text{A7})$$

and define $q_n(c | \tilde{\Theta}) := \frac{1}{Z_n} p(c | \mathbf{x}_n, \tilde{\Theta}) \delta(c \in \mathcal{K}^{(n)})$ and $q_{n,c}(\mathbf{z} | \tilde{\Theta}) := p(\mathbf{z} | c, \mathbf{x}_n, \tilde{\Theta})$. Z_n is a normalization constant given by

$$Z_n = \sum_{\tilde{c} \in \mathcal{K}^{(n)}} \int p(\tilde{c}, \mathbf{z} | \mathbf{x}_n, \tilde{\Theta}) d\mathbf{z} = \sum_{\tilde{c} \in \mathcal{K}^{(n)}} p(\tilde{c} | \mathbf{x}_n, \tilde{\Theta}) \int p(\mathbf{z} | \tilde{c}, \mathbf{x}_n, \tilde{\Theta}) d\mathbf{z} = \sum_{\tilde{c} \in \mathcal{K}^{(n)}} p(\tilde{c} | \mathbf{x}_n, \tilde{\Theta}).$$

The distribution $q_n(c | \tilde{\Theta})$ mirrors Eq. (4) in the main text, consistent with previous work employing truncated variational approximations for mixture models [e.g. 12, 13]. We recognize that $q_{n,c}(\mathbf{z} | \tilde{\Theta}) = p(\mathbf{z} | c, \mathbf{x}_n, \tilde{\Theta})$ conforms to a Gaussian distribution $\mathcal{N}(\mathbf{z}; \tilde{\boldsymbol{\mu}}_z, \tilde{\boldsymbol{\Sigma}}_z)$, with

$$\tilde{\boldsymbol{\Sigma}}_z = \left(\mathbf{I} + \tilde{\boldsymbol{\Lambda}}_c^\top \tilde{\mathbf{D}}_c^{-1} \tilde{\boldsymbol{\Lambda}}_c \right)^{-1} = \tilde{\mathbf{L}}_c^{-1}, \quad \tilde{\boldsymbol{\mu}}_z = \tilde{\boldsymbol{\Sigma}}_z \tilde{\boldsymbol{\Lambda}}_c^\top \tilde{\mathbf{D}}_c^{-1} (\mathbf{x}_n - \tilde{\boldsymbol{\mu}}_c) = \tilde{\mathbf{V}}_c (\mathbf{x}_n - \tilde{\boldsymbol{\mu}}_c).$$

In the following, we introduce the variational free energy and reformulate it into a more convenient form for deriving the parameter update equations. This free energy is given by

$$\mathcal{F}(\mathbf{x}_{1:N}; \mathcal{K}, \tilde{\Theta}, \Theta) = \sum_{n=1}^N \sum_{c=1}^C \int_{\mathbb{R}^H} q(c, \mathbf{z} | \mathbf{x}_n, \tilde{\Theta}) \log p(c, \mathbf{z}, \mathbf{x}_n | \Theta) d\mathbf{z} + \mathcal{H}[q],$$

where $\mathcal{H}[q] = -\sum_n \mathbb{E}_q[\log q(c, \mathbf{z} | \mathbf{x}_n, \tilde{\Theta})]$ denotes the Shannon entropy. Substituting Eq. (A7) into the free energy yields

$$\begin{aligned} \mathcal{F}(\mathbf{x}_{1:N}; \mathcal{K}, \tilde{\Theta}, \Theta) &= \sum_{n,c} q_n(c | \tilde{\Theta}) \int q_{n,c}(\mathbf{z} | \tilde{\Theta}) \log p(c, \mathbf{z}, \mathbf{x}_n | \Theta) d\mathbf{z} + \mathcal{H}[q] \\ &= \sum_{n,c} q_n(c | \tilde{\Theta}) \mathbb{E}_{q_{n,c}} [\log p(c, \mathbf{z}, \mathbf{x}_n | \Theta)] + \mathcal{H}[q]. \end{aligned}$$

The expectation $\mathbb{E}_{q_{n,c}} [\log p(c, \mathbf{z}, \mathbf{x}_n | \Theta)]$ can be expressed as

$$\begin{aligned} \mathbb{E}_{q_{n,c}} [\log p(c, \mathbf{z}, \mathbf{x}_n | \Theta)] &= \mathbb{E}_{q_{n,c}} [\log p(c | \Theta) + \log p(\mathbf{z} | \Theta) + \log p(\mathbf{x}_n | c, \mathbf{z}, \Theta)] \\ &= \log \pi_c - \frac{D}{2} \log(2\pi) + \frac{1}{2} \log |\mathbf{D}_c^{-1}| - \frac{1}{2} \mathbb{E}_{q_{n,c}} [(\mathbf{x}_n - \boldsymbol{\mu}_c - \boldsymbol{\Lambda}_c \mathbf{z})^\top \mathbf{D}_c^{-1} (\mathbf{x}_n - \boldsymbol{\mu}_c - \boldsymbol{\Lambda}_c \mathbf{z})] \\ &= \log \pi_c - \frac{D}{2} \log(2\pi) + \frac{1}{2} \log |\mathbf{D}_c^{-1}| - \frac{1}{2} \mathbb{E}_{q_{n,c}} [(\mathbf{x}_n - \hat{\boldsymbol{\Lambda}}_c \hat{\mathbf{z}})^\top \mathbf{D}_c^{-1} (\mathbf{x}_n - \hat{\boldsymbol{\Lambda}}_c \hat{\mathbf{z}})] \end{aligned} \quad (\text{A8})$$

where we combined $\mathbf{\Lambda}_c$ and $\boldsymbol{\mu}_c$ by defining

$$\hat{\mathbf{\Lambda}}_c := [\mathbf{\Lambda}_c \quad \boldsymbol{\mu}_c], \quad \hat{\mathbf{z}} := \begin{bmatrix} \mathbf{z} \\ 1 \end{bmatrix},$$

as we have $\hat{\mathbf{\Lambda}}_c \hat{\mathbf{z}} = \mathbf{\Lambda}_c \mathbf{z} + \boldsymbol{\mu}_c$. By making use of the symmetry of \mathbf{D}_c^{-1} , the cyclic property of the trace, and the linearity of $\mathbb{E}_{q_{n,c}}[\cdot]$, the expectation in Eq. (A8) reformulates to

$$\begin{aligned} \mathbb{E}_{q_{n,c}} \left[(\mathbf{x}_n - \hat{\mathbf{\Lambda}}_c \hat{\mathbf{z}})^\top \mathbf{D}_c^{-1} (\mathbf{x}_n - \hat{\mathbf{\Lambda}}_c \hat{\mathbf{z}}) \right] &= \mathbf{x}_n^\top \mathbf{D}_c^{-1} \mathbf{x}_n - 2 \mathbf{x}_n^\top \mathbf{D}_c^{-1} \hat{\mathbf{\Lambda}}_c \mathbb{E}_{q_{n,c}} [\hat{\mathbf{z}}] \\ &\quad + \text{tr} \left(\hat{\mathbf{\Lambda}}_c^\top \mathbf{D}_c^{-1} \hat{\mathbf{\Lambda}}_c \mathbb{E}_{q_{n,c}} \left[\hat{\mathbf{z}} \hat{\mathbf{z}}^\top \right] \right), \end{aligned}$$

Inserting the aforementioned results into the free energy yields

$$\begin{aligned} \mathcal{F}(\mathbf{x}_{1:N}; \mathcal{K}, \tilde{\boldsymbol{\Theta}}, \boldsymbol{\Theta}) &= \sum_{n,c} q_n(c | \tilde{\boldsymbol{\Theta}}) \left(\log \pi_c - \frac{D}{2} \log(2\pi) + \frac{1}{2} \log |\mathbf{D}_c^{-1}| - \frac{1}{2} \mathbf{x}_n^\top \mathbf{D}_c^{-1} \mathbf{x}_n \right. \\ &\quad \left. + \mathbf{x}_n^\top \mathbf{D}_c^{-1} \hat{\mathbf{\Lambda}}_c \mathbb{E}_{q_{n,c}} [\hat{\mathbf{z}}] - \frac{1}{2} \text{tr} \left(\hat{\mathbf{\Lambda}}_c^\top \mathbf{D}_c^{-1} \hat{\mathbf{\Lambda}}_c \mathbb{E}_{q_{n,c}} \left[\hat{\mathbf{z}} \hat{\mathbf{z}}^\top \right] \right) \right) + \mathcal{H}[q], \end{aligned} \quad (\text{A9})$$

where the expectation values $\mathbb{E}_{q_{n,c}}[\cdot]$ are given by

$$\mathbb{E}_{q_{n,c}} [\hat{\mathbf{z}}] = \begin{bmatrix} \tilde{\boldsymbol{\mu}}_z \\ 1 \end{bmatrix}, \quad \mathbb{E}_{q_{n,c}} \left[\hat{\mathbf{z}} \hat{\mathbf{z}}^\top \right] = \begin{bmatrix} \tilde{\boldsymbol{\Sigma}}_z + \tilde{\boldsymbol{\mu}}_z \tilde{\boldsymbol{\mu}}_z^\top & \tilde{\boldsymbol{\mu}}_z \\ \tilde{\boldsymbol{\mu}}_z^\top & 1 \end{bmatrix}.$$

Based on this expression of the free energy, we derive the update equations by equating the partial derivatives of Eq. (A9) w.r.t. all model parameters $\boldsymbol{\Theta}$ to zero, while keeping the variational parameters $\tilde{\boldsymbol{\Theta}}$ fixed.

Updates of mixing proportions: Considering the constraint $\sum_c \pi_c = 1$, the mixing proportions are determined by the well-known expression

$$\pi_c = \frac{N_c}{N} \quad \text{with} \quad N_c = \sum_n q_n(c | \tilde{\boldsymbol{\Theta}}). \quad (\text{A10})$$

Updates of means and factor loadings: For the derivative w.r.t. $\hat{\mathbf{\Lambda}}_c$ we obtain

$$\mathbf{0} = \frac{\partial \mathcal{F}}{\partial \hat{\mathbf{\Lambda}}_c} = \sum_n q_n(c | \tilde{\boldsymbol{\Theta}}) \mathbf{D}_c^{-1} \mathbf{x}_n \mathbb{E}_{q_{n,c}} [\hat{\mathbf{z}}]^\top - \sum_n q_n(c | \tilde{\boldsymbol{\Theta}}) \mathbf{D}_c^{-1} \hat{\mathbf{\Lambda}}_c \mathbb{E}_{q_{n,c}} \left[\hat{\mathbf{z}} \hat{\mathbf{z}}^\top \right],$$

resulting in

$$\begin{aligned} \sum_n q_n(c | \tilde{\boldsymbol{\Theta}}) \mathbf{x}_n \mathbb{E}_{q_{n,c}} [\hat{\mathbf{z}}]^\top &= \hat{\mathbf{\Lambda}}_c \sum_n q_n(c | \tilde{\boldsymbol{\Theta}}) \mathbb{E}_{q_{n,c}} \left[\hat{\mathbf{z}} \hat{\mathbf{z}}^\top \right] \\ \Leftrightarrow \mathbf{Y}_c &= \hat{\mathbf{\Lambda}}_c \mathbf{E}_c \\ \Leftrightarrow \hat{\mathbf{\Lambda}}_c &= \mathbf{Y}_c \mathbf{E}_c^{-1}. \end{aligned}$$

where we introduced the following two matrices:

$$\mathbf{E}_c = \sum_n q_n(c | \tilde{\boldsymbol{\Theta}}) \mathbb{E}_{q_{n,c}} \left[\hat{\mathbf{z}} \hat{\mathbf{z}}^\top \right], \quad \mathbf{Y}_c = \sum_n q_n(c | \tilde{\boldsymbol{\Theta}}) \mathbf{x}_n \mathbb{E}_{q_{n,c}} [\hat{\mathbf{z}}]^\top.$$

The factor loading matrix $\mathbf{\Lambda}_c$ is obtained from the first H columns of $\hat{\mathbf{\Lambda}}_c$, while the mean $\boldsymbol{\mu}_c$ is given by the last column of $\hat{\mathbf{\Lambda}}_c$.

Update of variance: Taking derivatives w.r.t. \mathbf{D}_c^{-1} , we derive

$$\mathbf{0} = \frac{\partial \mathcal{F}}{\partial \mathbf{D}_c^{-1}} = \frac{1}{2} \sum_n q_n(c | \tilde{\boldsymbol{\Theta}}) \left(\mathbf{D}_c - \mathbf{x}_n \mathbf{x}_n^\top + 2 \mathbf{x}_n \mathbb{E}_{q_{n,c}} [\hat{\mathbf{z}}]^\top \hat{\mathbf{\Lambda}}_c^\top - \hat{\mathbf{\Lambda}}_c \mathbb{E}_{q_{n,c}} [\hat{\mathbf{z}} \hat{\mathbf{z}}^\top] \hat{\mathbf{\Lambda}}_c^\top \right).$$

It follows that

$$\begin{aligned} \mathbf{D}_c N_c &= \sum_n q_n(c | \tilde{\boldsymbol{\Theta}}) \mathbf{x}_n \mathbf{x}_n^\top - 2 \left(\sum_n q_n(c | \tilde{\boldsymbol{\Theta}}) \mathbf{x}_n \mathbb{E}_{q_{n,c}} [\hat{\mathbf{z}}]^\top \right) \hat{\mathbf{\Lambda}}_c^\top + \hat{\mathbf{\Lambda}}_c \left(\sum_n q_n(c | \tilde{\boldsymbol{\Theta}}) \mathbb{E}_{q_{n,c}} [\hat{\mathbf{z}} \hat{\mathbf{z}}^\top] \right) \hat{\mathbf{\Lambda}}_c^\top \\ &= \sum_n q_n(c | \tilde{\boldsymbol{\Theta}}) \mathbf{x}_n \mathbf{x}_n^\top - 2 \mathbf{Y}_c \hat{\mathbf{\Lambda}}_c^\top + \hat{\mathbf{\Lambda}}_c \mathbf{E}_c \hat{\mathbf{\Lambda}}_c^\top, \end{aligned}$$

Substituting $\mathbf{Y}_c = \hat{\mathbf{\Lambda}}_c \mathbf{E}_c$ into the last term, we obtain

$$\mathbf{D}_c N_c = \sum_n q_n(c | \tilde{\boldsymbol{\Theta}}) \mathbf{x}_n \mathbf{x}_n^\top - \mathbf{Y}_c \hat{\mathbf{\Lambda}}_c^\top.$$

Finally, by applying the diagonal constraint each diagonal element σ_{cd}^2 of \mathbf{D}_c can be computed as follows

$$\begin{aligned} \sigma_{cd}^2 &= \frac{1}{N_c} \text{diag} \left(\sum_n q_n(c | \tilde{\boldsymbol{\Theta}}) \mathbf{x}_n \mathbf{x}_n^\top - \mathbf{Y}_c \hat{\mathbf{\Lambda}}_c^\top \right)_d \\ &= \frac{1}{N_c} \left(\sum_n q_n(c | \tilde{\boldsymbol{\Theta}}) x_{nd}^2 - \sum_h (\mathbf{Y}_c \odot \hat{\mathbf{\Lambda}}_c)_{d,h} \right), \end{aligned} \tag{A11}$$

where all non-diagonal elements are set to zero and $\hat{\mathbf{\Lambda}}_c$ are the updated parameters given by Eq. (A11). Here, $\text{diag}(\cdot)$ denotes a vector constructed by the main diagonal of a given matrix and \odot denotes element-wise multiplication.

Given that $q_n(c | \tilde{\boldsymbol{\Theta}})$ is zero for $c \notin \mathcal{K}^{(n)}$, the computational efficiency of the above equations can be improved by summing solely over non-zero $q_n(c | \tilde{\boldsymbol{\Theta}})$, as elaborated in Sec. 2.1 in the main text.

A.3 Proof of Proposition 1

Let \mathcal{K} be a given collection of index sets $\mathcal{K}_{1:N}$. We now choose an arbitrary n and replace an index $c \in \mathcal{K}^{(n)}$ by the index $\tilde{c} \notin \mathcal{K}^{(n)}$. We denote the resulting index set by $\tilde{\mathcal{K}}^{(n)}$, and the collection of index sets $\mathcal{K}_{1:N}$ with

$\mathcal{K}^{(n)}$ replaced by $\tilde{\mathcal{K}}^{(n)}$ we denote by $\tilde{\mathcal{K}}$. Now, we obtain:

$$\begin{aligned}
& \mathcal{F}(\tilde{\mathcal{K}}, \Theta) > \mathcal{F}(\mathcal{K}, \Theta) \\
\Leftrightarrow & \sum_{\substack{n'=1 \\ n' \neq n}}^N \log \left(\sum_{c' \in \mathcal{K}^{(n')}} p(c', \mathbf{x}_{n'} | \Theta) \right) + \log \left(\sum_{c' \in \tilde{\mathcal{K}}^{(n)}} p(c', \mathbf{x}_n | \Theta) \right) \\
& > \sum_{\substack{n'=1 \\ n' \neq n}}^N \log \left(\sum_{c' \in \mathcal{K}^{(n')}} p(c', \mathbf{x}_{n'} | \Theta) \right) + \log \left(\sum_{c' \in \mathcal{K}^{(n)}} p(c', \mathbf{x}_n | \Theta) \right) \\
\Leftrightarrow & \log \left(\sum_{c' \in \tilde{\mathcal{K}}^{(n)}} p(c', \mathbf{x}_n | \Theta) \right) > \log \left(\sum_{c' \in \mathcal{K}^{(n)}} p(c', \mathbf{x}_n | \Theta) \right) \\
\Leftrightarrow & \sum_{c' \in \tilde{\mathcal{K}}^{(n)} \setminus \{\tilde{c}\}} p(c', \mathbf{x}_n | \Theta) + p(\tilde{c}, \mathbf{x}_n | \Theta) > \sum_{c' \in \mathcal{K}^{(n)} \setminus \{c\}} p(c', \mathbf{x}_n | \Theta) + p(c, \mathbf{x}_n | \Theta) \\
\Leftrightarrow & p(\tilde{c}, \mathbf{x}_n | \Theta) > p(c, \mathbf{x}_n | \Theta),
\end{aligned}$$

where we have used strict concavity of the logarithm and $\tilde{\mathcal{K}}^{(n)} \setminus \{\tilde{c}\} = \mathcal{K}^{(n)} \setminus \{c\}$.

With the same argumentation, the free energy decreases if $p(\tilde{c}, \mathbf{x}_n | \Theta) < p(c, \mathbf{x}_n | \Theta)$. For $p(\tilde{c}, \mathbf{x}_n | \Theta) = p(c, \mathbf{x}_n | \Theta)$ the free energy trivially remains unchanged. \square

A.4 Estimation of Component-to-Component Distances and KL-Divergence

In this section, we further elaborate on the derivation of the KL-divergence approximation $D_{c\tilde{c}}$, which we use to find components \tilde{c} similar to component c (Eq. (12) in the main text). Afterwards, we compare $D_{c\tilde{c}}$ to a previously suggested distance estimate in Appendix A.4.1.

We start by considering idealized assumptions to derive $D_{c\tilde{c}}$ as an approximation of the KL-divergence. Importantly, however, $D_{c\tilde{c}}$ remains a valid expression for the estimation of similarity of components \tilde{c} to c also if the idealized assumptions are not fulfilled (which we will elaborate on further below). The numerical experiments in Sec. 3 in the main text verify the validity of $D_{c\tilde{c}}$ through the effective and efficient performance of the v-MFA algorithm.

Let us first assume that v-MFA has already converged to a large extent, i.e., we assume that the GMM parameters have already reached values that accurately represent the data components, and that the search spaces $\mathcal{S}^{(n)}$ include the most likely components for their data points \mathbf{x}_n . Furthermore, we assume that the data is appropriately modeled by a GMM (i.e., approximately Gaussian components), and that the components are well separated. Under these idealized conditions, we can assume that $D_{c\tilde{c}}$ given by Eq. (12) in the main text can approximate the KL-divergence relatively well for any components \tilde{c} similar to c .

To illustrate this, we first consider the finite sample approximation of the KL-divergence (Eq. (10) in the main text) using M samples of $p(\mathbf{x} | c, \Theta)$, which becomes exact for $M \rightarrow \infty$:

$$D_{\text{KL}} [p(\mathbf{x} | c, \Theta) || p(\mathbf{x} | \tilde{c}, \Theta)] \approx \frac{1}{M} \sum_{m=1}^M \log \frac{p(\mathbf{x}_m | c, \Theta)}{p(\mathbf{x}_m | \tilde{c}, \Theta)}, \quad \text{where } \mathbf{x}_m \sim p(\mathbf{x} | c, \Theta). \quad (\text{A12})$$

Secondly, for well separated components, model parameters close to convergence and data that is well-modeled by Gaussian components, the partitions \mathcal{I}_c of Eq. (11) in the main text will contain data points close to those

that would be generated by $p(\mathbf{x} | c, \Theta)$. Therefore, we can further approximate Eq. (A12) by:

$$D_{\text{KL}} [p(\mathbf{x} | c, \Theta) || p(\mathbf{x} | \tilde{c}, \Theta)] \approx \frac{1}{|\mathcal{I}_c|} \sum_{n \in \mathcal{I}_c} \log \frac{p(\mathbf{x}_n | c, \Theta)}{p(\mathbf{x}_n | \tilde{c}, \Theta)}. \quad (\text{A13})$$

Finally, we introduce the condition $\delta(\tilde{c} \in \mathcal{S}^{(n)})$, which ensures that only components \tilde{c} within the search spaces $\mathcal{S}^{(n)}$ are considered. The condition is important for computational efficiency, as it avoids additional computations of $p(\mathbf{x}_n | \tilde{c}, \Theta)$ that are not performed during the partial E-step. A disadvantage is that the approximation quality may decrease as potentially fewer data points \mathbf{x}_n are considered for the approximation. However, if the algorithm has sufficiently converged, the components \tilde{c} in the search spaces $\mathcal{S}^{(n)}$ of all data points with $n \in \mathcal{I}_c$ will be almost the same. In that case, $\delta(\tilde{c} \in \mathcal{S}^{(n)})$ will nearly always be equal to one, and we obtain:

$$D_{\text{KL}} [p(\mathbf{x} | c, \Theta) || p(\mathbf{x} | \tilde{c}, \Theta)] \approx \frac{1}{N_{c\tilde{c}}} \sum_{n \in \mathcal{I}_c} \log \frac{p(\mathbf{x}_n | c, \Theta)}{p(\mathbf{x}_n | \tilde{c}, \Theta)} \delta(\tilde{c} \in \mathcal{S}^{(n)}) = D_{c\tilde{c}}, \quad (\text{A14})$$

where $N_{c\tilde{c}} = \sum_{n \in \mathcal{I}_c} \delta(\tilde{c} \in \mathcal{S}^{(n)}) \approx \sum_{n \in \mathcal{I}_c} 1 = |\mathcal{I}_c|$.

For sufficiently similar components \tilde{c} in the sense of KL-divergences, the estimate $D_{c\tilde{c}}$ can therefore provide an accurate approximation of the KL-divergence. However, as the components \tilde{c} become increasingly dissimilar, the uncertainty regarding the accuracy of this approximation increases.

On the other hand, the estimate $D_{c\tilde{c}}$ can not be expected to approximate the KL-divergence accurately if the components are strongly overlapping. In such cases, the sets \mathcal{I}_c may not represent their respective components well, as each data point can only be assigned to a single component. However, $D_{c\tilde{c}}$ will by construction still result in small values as long as model parameters and search spaces $\mathcal{S}^{(n)}$ have sufficiently converged. In an extreme case of $p(\mathbf{x}_n | \tilde{c}, \Theta)$ being almost equal to $p(\mathbf{x}_n | c, \Theta)$, the summands in Eq. (A14) will be close to zero. As a consequence, similar components in the KL-divergence sense will also be similar in a ranking based on $D_{c\tilde{c}}$, although values of $D_{c\tilde{c}}$ may divert from the values of the KL-divergences.

Finally, for components \tilde{c} that are *very* irrelevant to c , we set the values of $D_{c\tilde{c}}$ to infinity, which would also not match the values of the KL-divergence. However, irrelevant components in the KL-divergence sense are anyway disregarded for the definition of sets g_c in Eq. (13) in the main text.

To summarize, $D_{c\tilde{c}}$ serves as an approximation for the KL-divergence between $p(\mathbf{x}_n | c, \Theta)$ and $p(\mathbf{x}_n | \tilde{c}, \Theta)$, which can be quite coarse. However, as the values of $D_{c\tilde{c}}$ are only used for ranking the similarity of components, coarse estimates are sufficient. Furthermore, $D_{c\tilde{c}}$ preserves sufficient information about the KL-divergence and, most importantly, it is efficiently computable.

A.4.1 Comparison to Variational E-Steps of Previous GMM Optimizations

Previous work using variational E-steps [12, 13] has not considered GMMs with intra-component correlations. Estimation of component-to-component distances has, however, been used before by Hirschberger et al. [12], who applied the estimate

$$d_{c\tilde{c}}^2 := -\frac{1}{N_{c\tilde{c}}} \sum_{n \in \mathcal{I}_c} \log p(\tilde{c}, \mathbf{x}_n | \Theta) \delta(\tilde{c} \in \mathcal{S}^{(n)}), \quad (\text{A15})$$

where $N_{c\tilde{c}}$ is defined as in Eq. (12) in the main text. The estimate $d_{c\tilde{c}}^2$ was then used as a ranking to define sets g_c analogously to Eq. (13) in the main text.

For isotropic components with equal variances and equal mixing proportions per component, it was argued that $d_{c\tilde{c}}^2$ will finally correspond to the Euclidean component-to-component distance (and $d_{c\tilde{c}}^2$ was originally defined

for this isotropic case). More concretely, it was shown (Appendix E of [12]) that $d_{c\tilde{c}}^2$ results in approximately the same distance ranking of component pairs (c, \tilde{c}) as the Euclidean component-to-component distance $\|\boldsymbol{\mu}_c - \boldsymbol{\mu}_{\tilde{c}}\|$. For diagonal covariance matrices, $d_{c\tilde{c}}^2$ was also related to KL-divergences.

From the perspective of the here used approach in Eq. (12) in the main text, however, Eq. (A15) can be considered as ignoring $p(\mathbf{x}_n | c, \boldsymbol{\Theta})$ in the KL-divergence (Eq. (10) in the main text). A further difference is a different consideration of the mixing proportions. Estimate Eq. (A15) has been shown to perform well for isotropic and diagonal components [12], for which it was originally derived. Here, we directly derived from KL-divergences, which implicitly accounts for different intra-component correlations. Consequently, the more general derivation of $D_{c\tilde{c}}$ (used for v-MFA) is a better match to these intra-component correlations, and hence can be expected to result in a more efficient learning algorithm. If and how much the more general estimate Eq. (12) in the main text is improving learning remains to be numerically investigated, which we provide in Appendix B.2.1.

A.5 Algorithmic Complexity of the Variational E-step

To determine the algorithmic complexity of Alg. 1 in the main text, we analyze each of its four blocks, assuming $N > C$. Alg. 3 outlines the steps in Alg. 1 in the main text along with the complexity of each block (emphasized in bold) and the intermediate steps.

Block 1: This block begins with constructing the search space, where each search space can contain up to $S = C'G + 1$ elements. Following this, the joints are computed, whereas each joint computation has a complexity of $\mathcal{O}(DH)$ (see Appendix A.1). Next, selecting the C' largest values among the computed joints to obtain $\mathcal{K}^{(n)}$ for a data point can be performed in $\mathcal{O}(S)$ [54]. Since we need to evaluate up to S joints per data point, the overall complexity of block 1 is $\mathcal{O}(NSDH)$.

Block 2: In block 2, the dataset is partitioned into $\mathcal{I}_{1:C}$. To find the most likely component c_n within the $\mathcal{K}^{(n)}$ set of each data point, the component with the largest joint is selected, which has a complexity of $\mathcal{O}(C')$. Repeating this for all data points results in a total complexity of $\mathcal{O}(NC')$.

Block 3: By construction, the union of all \mathcal{I}_c contains all indices of the N data points exactly once. Therefore, in block 3, we loop over each search space of the data points exactly once, resulting in complexity of $\mathcal{O}(NS)$. On average, \mathcal{I}_c contains N/C indices. Thus, the average cost to iterate over all n in \mathcal{I}_c and the respective $\mathcal{S}^{(n)}$ is $\mathcal{O}^\dagger((N/C)S)$. Similar to the update of $\mathcal{K}^{(n)}$ in block 1, the complexity of finding G replacement candidates to obtain g_c is $\mathcal{O}^\dagger((N/C)S)$ on average.

Block 4: Normalizing the variational distributions requires calculating the normalization constant Z_n by summing over all C' indices in $\mathcal{K}^{(n)}$, followed by dividing by Z_n . Consequently, the total computational complexity for all data points is $\mathcal{O}(NC')$.

Summarizing the complexities of all four blocks, the overall algorithmic complexity of Alg. 3 is $\mathcal{O}(NSDH + NC' + NS + NC') = \mathcal{O}(NSDH)$.

Alg. 3 is analogous to the partial variational E-step described in [12], with three differences. We will discuss these differences below, focusing on the complexity of the respective algorithms. First, we refrain from using coresets. In [12], the use of coresets reduces the complexity from N to the coreset size N' , where $N > N'$. But coresets are not desirable in our setting, as discussed in Sec. 1 in the main text. Second, computing a joint defined by the MFA model requires $\mathcal{O}(HD)$ operations, in contrast to the $\mathcal{O}(D)$ operations required for the GMMs considered in [12]. The additional cost allows for a much more flexible modeling of correlations (i.e., of component shapes) than GMMs restricted to uncorrelated data per component. Nevertheless, a quadratic scaling with D (as would be required for full covariance matrices) is avoided. Third, the update of variational parameters via the estimation of component similarity is different (see Sec. 2.3 in the main text, Appendix A.4.1 and Appendix B.2.1).

Algorithm 3: Complexity of the Variational E-step

for $n = 1 : N$ do	$\mathcal{S}^{(n)} = \bigcup_{c \in \mathcal{K}^{(n)}} g_c;$	$\mathcal{O}(NSDH)$
	$\mathcal{S}^{(n)} = \mathcal{S}^{(n)} \cup \{c\}$ with $c \sim \mathcal{U}\{1, C\};$	$\mathcal{O}(S)$
1	for $c \in \mathcal{S}^{(n)}$ do	$\mathcal{O}(1)$
	└ compute joint $p(c, \mathbf{x}_n \Theta);$	$\mathcal{O}(SDH)$
	└ $\mathcal{K}^{(n)} = \{c p(c, \mathbf{x}_n \Theta) \text{ is among the } C' \text{ largest joints for all } c \in \mathcal{S}^{(n)}\};$	$\mathcal{O}(DH)$
		$\mathcal{O}(S)$
<hr/>		
for $n = 1 : N$ do	$c_n = \operatorname{argmax}_{c \in \mathcal{K}^{(n)}} p(c, \mathbf{x}_n \Theta);$	$\mathcal{O}(NC')$
2	└ $\mathcal{I}_{c_n} = \mathcal{I}_{c_n} \cup \{n\};$	$\mathcal{O}(C')$
		$\mathcal{O}(1)$
<hr/>		
for $c = 1 : C$ do	for $n \in \mathcal{I}_c$ do	$\mathcal{O}(NS)$
	└ for $\tilde{c} \in \mathcal{S}^{(n)} \setminus \{c\}$ do	$\mathcal{O}^\dagger((N/C)S)$
	└ └ $\tilde{D}_{c\tilde{c}} = \tilde{D}_{c\tilde{c}} + \log p(\mathbf{x}_n c, \Theta) - \log p(\mathbf{x}_n \tilde{c}, \Theta);$	$\mathcal{O}(S)$
3	└ └ $N_{c\tilde{c}} = N_{c\tilde{c}} + 1;$	$\mathcal{O}(1)$
	└ └ $\mathcal{D}_c = \mathcal{D}_c \cup \{\tilde{c}\};$	$\mathcal{O}(1)$
	└ for $\tilde{c} \in \mathcal{D}_c$ do	$\mathcal{O}^\dagger((N/C)S)$
	└ └ $D_{c\tilde{c}} = \tilde{D}_{c\tilde{c}} / N_{c\tilde{c}};$	$\mathcal{O}(1)$
	└ $g_c = \{\tilde{c} D_{c\tilde{c}} \text{ is among the } G - 1 \text{ smallest values for } \tilde{c} \in \mathcal{D}_c\} \cup \{c\};$	$\mathcal{O}^\dagger((N/C)S)$
<hr/>		
for $n = 1 : N$ do	for $c \in \mathcal{K}^{(n)}$ do	$\mathcal{O}(NC')$
	└ $Z_n = Z_n + p(c, \mathbf{x}_n \Theta);$	$\mathcal{O}(C')$
4	for $c \in \mathcal{K}^{(n)}$ do	$\mathcal{O}(1)$
	└ $q_n(c \Theta) = p(c, \mathbf{x}_n \Theta) / Z_n;$	$\mathcal{O}(C')$
		$\mathcal{O}(1)$

\mathcal{O}^\dagger denotes amortized or average complexity

B Supporting Information on Numerical Experiments and Control Experiments

In the following, we provide further specifics on the implementation and execution of the algorithms, the used hardware and the datasets in Appendix B.1, results of additional control experiments in Appendix B.2 and supplementary information on the quality analysis in Appendix B.3.

B.1 Further Details on Numerical Experiments

Below, we present additional details regarding the implementation and execution of the algorithms as well as information about the used hardware and the datasets.

B.1.1 Algorithms

The em-MFA and the v-MFA algorithms are our own implementations. To ensure a fair comparison, the primary motivation behind developing these algorithms was to optimize for execution speed and efficient memory usage. The *torch-mfa* algorithm is a published PyTorch-based implementation of MFA that uses Stochastic Gradient Descent (SGD). The *k-means+FA* algorithm combines *k-means* with factor analysis. While it was used as an initialization method in [18], we employ it here as a comparison method to the other algorithms.

v-MFA: The v-MFA algorithm trains the MFA model using the variational EM algorithm described in Secs. 2.1 to 2.4 in the main text. The implementation uses both Python and C++. The core functionality is written in C++, utilizing the open-source libraries Eigen [55] and Boost [56]. To facilitate data communication between Python and C++, pybind11 [57] is used. The v-MFA source code is available upon reasonable request for this preliminary version of the paper, and will be made publicly available via GitHub with the final version. The implementations of v-MFA^{Eucl.}, v-ISO and v-ISO^{Eucl.} used in Appendix B.2 are also provided in this source code.

em-MFA: Our Python implementation of the em-MFA algorithm optimizes the MFA model using exact inference via conventional EM (full posteriors). It primarily leverages the open-source library PyTorch [58]. The em-MFA source code is available upon reasonable request for this preliminary version of the paper, and will be made publicly available via GitHub with the final version.

k-means+FA: In this integrated methodology, the initial step entails the application of the *k-means* algorithm to the dataset. Upon convergence, the data is partitioned into Voronoi cells, with each data point \mathbf{x}_n assigned to its closest cluster (component) c , i.e.,

$$\mathcal{P}_c = \{n \mid c = c_n\} \quad \text{with} \quad c_n = \underset{c'}{\operatorname{argmin}} \|\mathbf{x}_n - \boldsymbol{\mu}_{c'}\|^2 \quad (\text{B1})$$

A factor analyzer is then applied to each data subset \mathcal{P}_c , where each factor analyzer independently learns the parameters $\boldsymbol{\mu}_c$, \mathbf{A}_c and \mathbf{D}_c for the corresponding cluster c . The priors π_c are determined based on the relative subset sizes, i.e.,

$$\pi_c = \frac{|\mathcal{P}_c|}{N}, \quad (\text{B2})$$

where N is the number of the total data points. The *k-means+FA* algorithm is realized by using the Scikit-learn [59] implementations (version 1.5.0) of *k-means* and Factor Analyzer, using their default hyperparameters and settings.

torch-mfa: We used the official *torch-mfa* [60] implementation, an advancement of the stochastic gradient descent (SGD) based MFA used in [18]. Due to the SGD optimization, *torch-mfa* introduces additional

parameters, such as learning rate and batch size. We set the batch size to 256, consistent with [18], and determined the optimal learning rate to be 10^{-2} via a coarse grid search (prior to the experiments). We modified the function `sgd_mfa_train` in the `mfa.py` script to implement a convergence criterion similar to Eq. (15) in the main text. The original function does a fixed number of iterations. Unlike em-MFA and v-MFA, where the free energy is computed for the entire dataset during each E-step, *torch-mfa* updates parameters after each batch, making full dataset evaluation impractical. Instead, we computed the free energy on a randomly selected subset of the dataset after each epoch and used this for the convergence criterion in Eq. (15) in the main text. The subset size was set to $10\times$ the batch size, and the computational time for this evaluation was excluded from the time measurement.

AFK-MC²: We provide an efficient implementation of the AFK-MC² seeding method [34] integrated into v-MFA. For all experiments, the Markov chain length was set to 10.

B.1.2 Hardware

Tab. B1 provides a detailed description of the hardware used for the various algorithms and experimental setups. To achieve high utilization, we executed four instances of v-MFA, em-MFA, or *k*-means+*FA* in parallel, with each instance using 16 of the 64 available cores, i.e., four independent runs were executed at the same time. The tool `GNU parallel` [61] was employed for job scheduling. An exception to this is the training of v-MFA on YFCC100M in Sec. 3.3 in the main text, where we executed only one instance at a time due to memory constraints, using all 64 available cores. We executed *torch-mfa* on a NVIDIA H100 GPU equipped with 96GB of VRAM. Running *torch-mfa* on the CPU configurations used by the other algorithms resulted in significantly longer execution times (GPU \approx 1 h vs. CPU (16 cores) $>$ 10 h for a single epoch).

Algorithm	Hardware		
	Device	Model name	Cores used
v-MFA	CPU	AMD Genoa EPYC 9554	16*
v-MFA on YFCC100M	CPU	AMD Genoa EPYC 9554	64
em-MFA	CPU	AMD Genoa EPYC 9554	16*
<i>k</i> -means+ <i>FA</i>	CPU	AMD Genoa EPYC 9554	16*
<i>torch-mfa</i>	GPU	NVIDIA H100 94GB SXM	all

Table B1: Details on the utilized hardware for the different algorithms and experiments. The asterisk (*) marks execution of four instances in parallel, with each instance using 16 of the 64 available cores, i.e., four independent runs were executed at the same time.

B.1.3 Datasets and Preprocessing

In the following, we provide additional information on the datasets used in the numerical experiments. Unless otherwise stated, we use the official *train* and *test* splits, and the images are used as provide by there sources without preprocessing. Note that the label information was not used in any of the experiments.

CIFAR-10: The CIFAR-10 dataset [41] consists of 60 000 natural color images with size 32×32 , divided into 50 000 training images and 10 000 test images.

CelebA: The original CelebA dataset [42] contains 202 599 color images of faces sized at 178×218 . We preprocessed the data to align, crop and resize the images to 64×64 , following [18]. Additionally, we merged the *train* and *valid* splits to obtain more training data.

EMNIST: The EMNIST dataset [43] contains of small cropped grayscale images of handwritten digits and letters, sized at 28×28 . The images are split into different groups. We used the *byclass* split, which contains

697 932 training images and 116 323 test images. To avoid zero variances at the image edges, standard Gaussian noise (with zero mean and standard deviation of 1) was added to the images.

SVHN: Similar to the digits in EMNIST, the SVHN dataset [44] contains images of small cropped digits in the range from 0 to 9. But in contrast to EMNIST, these images are real, colored photographs capturing house numbers at a size of 32×32 . The SVHN dataset is split into 73 257 training images (*train*), 26 032 test images (*test*) and 531 131 additional training images (*extra*). To obtain more training data, we merged the *extra* and *train* images.

YFCC100M: The original YFCC100M dataset [45] contains real-world images and videos. We used all available images; some of the the original 99 171 688 images were missing or corrupted and thus not included. The remaining 99 155 298 images of various sizes were center-cropped and resized with bilinear interpolation to 32×32 . We randomly selected a test split of 4 957 765 samples (5% of the dataset) and used the remaining 94 197 533 samples for training.

B.2 Numerical Control Experiments

The following subsections report the results of additional control experiments, offering supporting or complementary insights to those discussed in Sec. 3 in the main text.

B.2.1 Comparison of Component-to-Component Distance Estimates

In this section, we compare our v-MFA algorithm, which uses the proposed definition of g_c based on the estimate $D_{c\bar{c}}$ in Eq. (12) in the main text, with a variant of v-MFA (referred to as v-MFA^{Eucl.}) that uses the definition of g_c introduced in [12], based on $d_{c\bar{c}}^2$ in Eq. (A15). In addition to the MFA model, we also consider isotropic GMMs (compare Eq. (5) in [12]) and their optimization using variational EM with g_c based on $D_{c\bar{c}}$ (referred to as v-ISO) and with g_c based on $d_{c\bar{c}}^2$ (referred to as v-ISO^{Eucl.}). v-ISO^{Eucl.} is the algorithm used in previous work [12].

We numerically compare v-MFA and v-MFA^{Eucl.} to investigate the differences of the here derived approach to the previous approach. Additionally, we compare v-ISO to v-ISO^{Eucl.} to investigate potential advantages and disadvantages under the constraint of isotropic components.

The models are initialized identically and using the same settings as described in Sec. 3.2 and Fig. 5 in the main text. Since both methods use partial E-Steps with the same computational complexity, we run the algorithms for a fixed number of iterations. Concretely, we train v-MFA (or v-ISO) until convergence, and then train v-MFA^{Eucl.} (or v-ISO^{Eucl.}) for the same number of iterations.

The comparison results for the MFA models and for the isotropic GMMs are presented in Fig. B1 and Fig. B2, respectively. In the case of MFAs, the here derived v-MFA algorithm consistently performs better (or comparable within the error bars) in terms of NLL_{test} values when compared to v-MFA^{Eucl.} (especially for smaller search spaces $\mathcal{S}^{(n)}$). As the search space expands, the NLL_{test} values of both algorithms approach each other.

Also in the case of GMMs with isotropic components, v-ISO improves on NLL_{test} values compared to v-ISO^{Eucl.} albeit at a slightly higher computational cost, due to smaller intersections in the search spaces. Notably, v-ISO^{Eucl.} only differs slightly from v-ISO in terms of NLL_{test} values for most of the datasets and settings of C' and G (see Fig. B2), which confirms the suitability $d_{c\bar{c}}^2$ of Eq. (A15) for the isotropic case, for which it was originally derived [12]. In contrast, in the case of GMMs with flexible covariances (i.e., for the MFA model), the significant improvements of v-MFA compared to v-MFA^{Eucl.} highlight the importance of the more general definition of g_c using $D_{c\bar{c}}$ given by Eq. (12) in the main text.

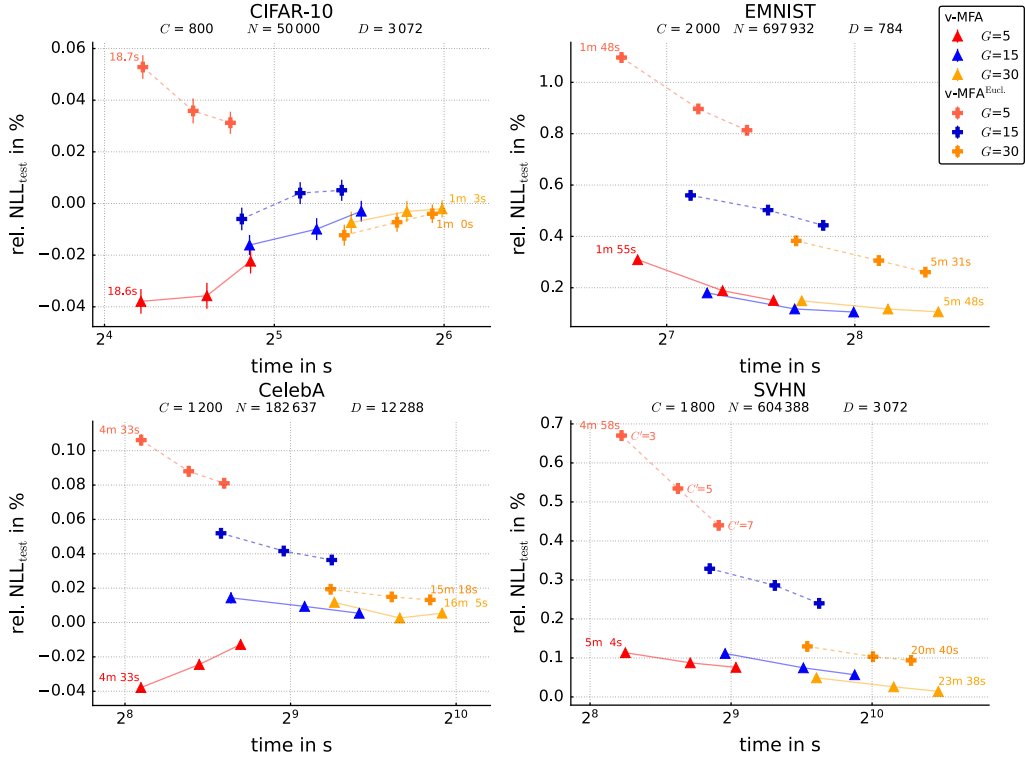


Figure B1: Effectiveness and efficiency of v-MFA and v-MFA^{Eucl.} in terms of NLL_{test} (relative to em-MFA) and the runtime. Triangles refer to v-MFA, while pluses denote v-MFA^{Eucl.}. Each of the four subfigures corresponds to experiments on one benchmark dataset. The settings are similar to those in Fig. 5 in the main text, but both algorithms are trained for the same number of iterations, as detailed in the text. For each configuration of $G \in \{5, 15, 30\}$, measurements refer to configurations with $C' \in \{3, 5, 7\}$ (three red, blue and orange triangles or pluses, respectively). Configurations with larger C' lie to the right, due to their longer runtimes. Each measurement point is averaged over 40 independent runs and error bars denote the standard error of the mean (SEM).

B.2.2 Comparison to other Implementations

In experiments in Sec. 3.1 and Sec. 3.2 in the main text, we showed the speed-up of our variationally accelerated algorithm (v-MFA) compared to conventional EM optimization for MFA (em-MFA). To ensure a fair comparison, the primary motivation for developing v-MFA and em-MFA was to optimize execution speed. To investigate their efficiency against existing algorithms in the literature, we compared them with an already published implementation of MFA optimization [18] which is based on stochastic gradient descent (SGD) (but is not using variational acceleration). Concretely, we used the *torch-mfa* algorithm which is based on the PyTorch framework and uses its integrated optimizers for SGD. *torch-mfa* represents a further advancement of the TensorFlow implementation employed to produce the previously reported results [18] (for further details, see Appendix B.1.1). To the best of the authors knowledge, the work by [18] documented the largest MFA models prior to our study. However, at the scales we here address, one can observe clear efficiency limits of *torch-mfa* (as well as its predecessor implementation), which we elaborate on further below.

When considering time measurements for the various settings, note that although actual runtimes have significant practical relevance, they are inherently dependent on implementation details and hardware. We do not

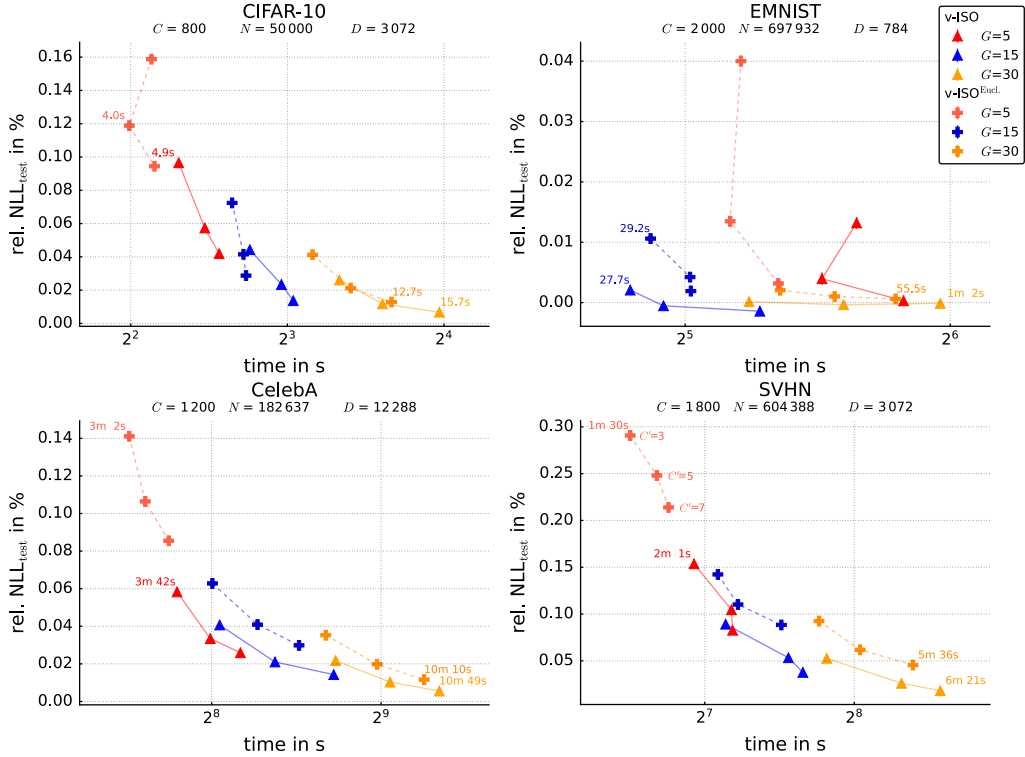


Figure B2: Effectiveness and efficiency of v-ISO and v-ISO^{Eucl.} in terms of NLL_{test} (relative to em-MFA) and the runtime. Triangles refer to v-ISO, while pluses denote v-ISO^{Eucl.}. Each of the four subfigures corresponds to experiments on one benchmark dataset. The settings are similar to those in Fig. 5 in the main text, but both algorithms are trained for the same number of iterations, as detailed in the text. For each configuration of $G \in \{5, 15, 30\}$, measurements refer to configurations with $C' \in \{3, 5, 7\}$ (three red, blue and orange triangles or pluses, respectively). Each measurement point is averaged over 40 independent runs and error bars denote the standard error of the mean (SEM).

claim, nor do we expect, that *torch-mfa* is optimal in any specific sense, but rather representative of what a typical implementation might achieve.

To assess the performance of *torch-mfa* against v-MFA and em-MFA, we adopted the configurations used in an experiment on the CelebA dataset (see [18]). The number of components and the hyperplane dimension are set to $C = 1000$ and $H = 10$ for all algorithms. We ran *torch-mfa* on a GPU with the configurations specified in Appendix B.1. This is in contrast to the CPU configurations for the other algorithm, as discussed in Appendix B.1.2. The experiments in [18] were performed utilizing hierarchical training (for more details we refer to [18]). To ensure a fair comparison, we trained *torch-mfa* in our experiments directly on the complete dataset, without hierarchical training. In addition to *torch-mfa*, v-MFA and em-MFA, we used the *k*-means+FA algorithm in for our experimental comparison. The results are shown in Tab. B2.

Table B2: Comparison of em-MFA, v-MFA, k -means+FA and *torch-mfa* on CelebA with $C = 1000$. To ensure consistency with the other methods, we define an iteration for *torch-mfa* as completed when the model has processed the entire dataset, rather than just one data batch. Results are averaged over 4 independent runs. All errors indicate the standard error of the mean (SEM), rounded up to the displayed precision. The best values for NLL_{test} , the relative NLL_{test} , runtime (d=days, h=hours, m=minutes, s=seconds) and the number of joint or distance evaluations are marked bold.

	NLL_{test}	rel. NLL_{test}	runtime	joint / distance eval.	iterations
em-MFA	57571 ± 3	0.00 %	1h 16m \pm 53.5s	$(4.66 \pm 0.05) \cdot 10^9$	25.5
v-MFA	57565 ± 2	$(-0.01 \pm 0.01) \%$	9m 2s \pm 11.6s	$(2.47 \pm 0.05) \cdot 10^8$	35.0
k -means+FA	58373 ± 2	$(1.39 \pm 0.00) \%$	12m 12s \pm 2.8s	$(1.83 \pm 0.01) \cdot 10^{10}$	106.7
<i>torch-mfa</i>	57868 ± 13	$(0.52 \pm 0.02) \%$	1d 14h \pm 1h 35m	$(6.8 \pm 0.3) \cdot 10^9$	38.5

The findings show that v-MFA achieved the lowest NLL_{test} value in comparison to the other algorithms, with NLL values that are essentially equal to those of em-MFA. In terms of computational efficiency, v-MFA was clearly the fastest algorithm, completing in approximately 9 minutes. Following closely behind is k -means+FA, with a runtime of approximately 12 minutes. The em-MFA algorithm exhibited considerably worse runtime performance, necessitating over 1 hour to complete. Remarkably, the *torch-mfa* algorithm was the most time-consuming, requiring approximately one and a half days to complete, making it the slowest among the algorithms.

A possible reason for the long runtimes of *torch-mfa* could be related to the optimization procedure. Unlike the other algorithms, which update model parameters once per iteration (M-step evaluated over the entire dataset), *torch-mfa* updates parameters after each data batch. Consequently, this results in approximately $\frac{N}{\text{batch size}} = \frac{182637}{256} \approx 713 \times$ as many (yet less computationally expensive) parameter updates. In this context, we attempted to increase the batch size (to 512) in order to potentially reduce the runtime. However, this was not possible due to memory constraints of the used GPU. Another factor to consider is that the design objectives of the em-MFA and v-MFA algorithms were mainly focused on optimizing speed, whereas speed might not have been the main objective for the *torch-mfa* algorithm.

In terms of the number of joint or distance evaluations, v-MFA also exhibited the lowest value with an order of magnitude fewer evaluations than em-MFA and *torch-mfa*, which were within the same order of magnitude. The greatest number of distance evaluations was performed by k -means+FA, once more an order of magnitude higher than those of em-MFA and *torch-mfa*. This observation seems to be inconsistent with the runtimes of the algorithms. However, a distance evaluation of k -means is significantly less computationally expensive than a joint evaluation of the other algorithms.

B.2.3 Control Experiments for the v-MFA Scalability Analysis

The results in Fig. 4 in the main text do not account for the quality of em-MFA and v-MFA. However, it is important to consider the optimization quality also for the investigation of scaling behavior because the improved scaling of v-MFA may be attributed to two key factors: First, the variational approach reduces the computational complexity of the algorithm, which is the desired effect we aim to measure. Second, there is typically a loss in quality as v-MFA approximate the conventional EM optimization of em-MFA.

Therefore, we conducted controls by repeating the experiments in Sec. 3.1 in the main text, now incorporating the different modeling qualities measured by the NLL on the test datasets. Concretely, we stopped the em-MFA algorithm once it achieved the same NLL_{test} as the v-MFA algorithm upon convergence. In practice, however, the NLL_{test} values of the em-MFA and the v-MFA algorithms are not expected to reach identical values.

To address this, we proceeded as follows: We trained the em-MFA algorithm while monitoring the NLL_{test} during training. When the NLL_{test} of em-MFA surpassed that of v-MFA, we stopped the algorithm. We then used the model parameters from the *previous* iteration to ensure that the quality of em-MFA was approximately the same as (but slightly worse than) the quality of v-MFA. The results of this procedure are denoted as em-MFA[†] in Fig. B3, i.e., em-MFA[†] shows the speed-up achievable if em-MFA is only required to achieve the final optimization quality of v-MFA. All other results shown in Fig. B3 are taken from Fig. 4 in the main text.

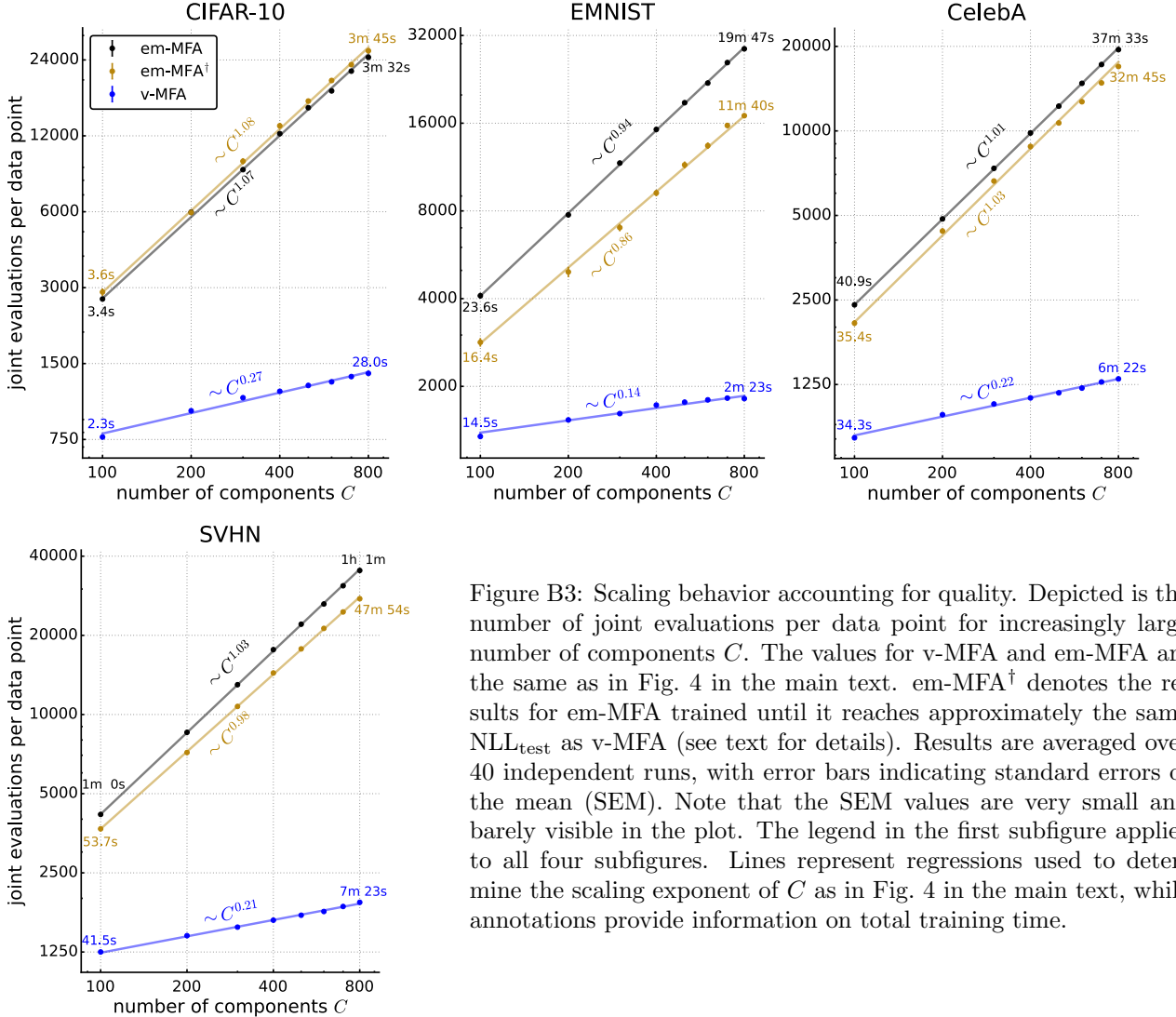


Figure B3: Scaling behavior accounting for quality. Depicted is the number of joint evaluations per data point for increasingly large number of components C . The values for v-MFA and em-MFA are the same as in Fig. 4 in the main text. em-MFA[†] denotes the results for em-MFA trained until it reaches approximately the same NLL_{test} as v-MFA (see text for details). Results are averaged over 40 independent runs, with error bars indicating standard errors of the mean (SEM). Note that the SEM values are very small and barely visible in the plot. The legend in the first subfigure applies to all four subfigures. Lines represent regressions used to determine the scaling exponent of C as in Fig. 4 in the main text, while annotations provide information on total training time.

For two of the four datasets, em-MFA[†] achieved a smaller scaling exponent than em-MFA. The number of iterations required to obtain the same NLL_{test} as v-MFA decreases slightly with increasingly large values of C . For both CIFAR-10 and CelebA, the scaling exponents of em-MFA[†] and em-MFA are approximately the same. On CIFAR-10, the NLL_{test} values of v-MFA are lower than those of em-MFA for sufficiently large values of C , as also observed in Fig. 5 in the main text. Consequently, the algorithm requires more iterations than previously to reach the desired quality.

Overall, the scaling exponent of v-MFA remains significantly lower than that of em-MFA[†] across all four datasets. The control experiments thus show that the improved scaling behavior of v-MFA can be attributed to the sublinear complexity of the algorithm, while the impact of reduced quality contributes only a small fraction to the effect or is negligible.

B.3 Additional information on the quality analysis

Additional information and results about the experiments in Sec. 3.2 in the main text are provided in Tab. B3. The table reports the relative NLL_{test} , the average speed-up in terms of runtime and joint evaluations (or distance evaluations for k -means+ FA) compared to em-MFA as well as the median number of iterations until convergence. Additionally, for the v-MFA algorithm, the *warm-up* iterations are reported (note that the total number of iterations includes the *warm-up* iterations).

Table B3: Additional information and results for the experiments in Sec. 3.2 in the main text. Standard errors of the mean (SEM) for relative NLL_{test} were below 0.01%.

Dataset #Components	Algorithm Name	C'	G	rel. NLL_{test}	Rel. speed-up		#Iterations	
					Time	Joints/Dist.	warm-up	total
CIFAR-10 $C = 800$	em-MFA	-	-	0.0%	1.0×	1.0×	-	31.0
	k -means+FA	-	-	1.64%	4.4×	0.5×	-	77.6
	v-MFA	3	5	-0.04%	11.5×	29.8×	15.0	52.0
		3	15	-0.02%	7.4×	17.2×	7.0	39.0
		3	30	-0.01%	4.9×	10.7×	5.0	37.0
		5	5	-0.04%	8.8×	22.3×	12.0	45.5
		5	15	-0.01%	5.6×	12.9×	6.0	37.0
		5	30	-0.00%	3.9×	8.4×	4.0	35.5
		7	5	-0.02%	7.3×	18.2×	10.0	42.0
		7	15	-0.00%	4.7×	10.6×	6.0	37.0
7	30	-0.00%	3.4×	7.2×	4.0	35.0		
EMNIST $C = 2000$	em-MFA	-	-	0.0%	1.0×	1.0×	-	29.0
	k -means+FA	-	-	7.48%	5.5×	0.3×	-	112.6
	v-MFA	3	5	0.31%	19.3×	41.9×	37.0	87.0
		3	15	0.18%	14.9×	30.1×	16.0	48.0
		3	30	0.15%	10.5×	20.7×	8.0	38.5
		5	5	0.19%	14.1×	30.6×	31.0	75.0
		5	15	0.12%	10.8×	21.8×	13.0	43.0
		5	30	0.12%	7.7×	15.0×	8.0	37.0
		7	5	0.15%	11.7×	25.2×	27.0	67.0
		7	15	0.11%	8.7×	17.4×	11.0	40.0
7	30	0.11%	6.4×	12.4×	6.0	35.0		
CelebA $C = 1200$	em-MFA	-	-	0.0%	1.0×	1.0×	-	24.0
	k -means+FA	-	-	1.03%	3.3×	0.2×	-	108.6
	v-MFA	3	5	-0.04%	11.8×	30.7×	20.0	57.0
		3	15	0.01%	8.1×	20.3×	8.0	35.0
		3	30	0.01%	5.3×	12.9×	6.0	31.0
		5	5	-0.02%	9.3×	23.5×	15.0	48.0
		5	15	0.01%	6.0×	14.7×	6.0	32.0
		5	30	0.00%	4.0×	9.7×	5.0	29.0
		7	5	-0.01%	7.8×	19.5×	13.0	42.0
		7	15	0.01%	4.7×	11.6×	6.0	30.5
7	30	0.01%	3.3×	8.1×	4.0	28.0		
SVHN $C = 1800$	em-MFA	-	-	0.0%	1.0×	1.0×	-	42.0
	k -means+FA	-	-	3.19%	7.0×	0.4×	-	110.3
	v-MFA	3	5	0.11%	25.6×	61.9×	17.0	78.0
		3	15	0.11%	15.7×	34.3×	8.0	54.0
		3	30	0.05%	10.0×	21.2×	6.0	50.0
		5	5	0.09%	18.6×	44.6×	13.0	68.0
		5	15	0.07%	10.7×	23.3×	7.0	51.0
		5	30	0.03%	6.8×	14.5×	6.0	49.0
		7	5	0.08%	14.9×	35.4×	11.0	63.0
		7	15	0.06%	8.3×	18.0×	6.0	50.0
7	30	0.01%	5.5×	11.6×	5.0	47.0		